Seismic Isolation of Surface Foundations Exploiting the Properties of Natural Liquefiable Soil

Xenia Karatzia[a,1], George Mylonakis[b] and George Bouckovalas[c]

[a] Geotechnical Engineer, PhD, Department of Civil Engineering, University of Patras, Rio 26500, Greece, xkar@upatras.gr
[b] Professor, Dept. of Civil Engineering, Univ. of Bristol, Queens Building, Bristol BS8 1TR, U.K.; Professor, Dept. of Civil Engineering, Univ. of Patras, Rio 26500, Greece; Adjunct Professor, Univ. of California at Los Angeles, CA 90095, g.mylonakis@bristol.ac.uk
[c] Professor, School of Civil Engineering, NTUA, Greece, gbouck@central.ntua.gr

[1] *Present address: HOCHTIEF Eng. GmbH Consult IKS, Lyoner Str. 25, 60528 Frankfurt am Main, Germany, polyxeni.karatzia@hochtief.de*

Abstract

A novel design method has recently been proposed for the seismic protection of structures on liquefied ground using shallow (instead of deep) foundations. Contrary to conventional (structural) isolation approaches, which employ special mechanical devices, the proposed (geotechnical) means exploits the presence of natural liquefiable soil, after partial remediation of the surface ground, as a natural base isolation system which de-amplifies the seismic ground motion and, hence, reduces the seismic demand on the superstructure. This paper focuses on the comparative evaluation of the relevant Soil-Foundation-Structure Interaction (SFSI) effects. Using an equivalent-linear approach based on appropriate values for the material properties of liquefied soil, the dynamic stiffness and damping of rigid square footings on three-layer liquefiable soil under external harmonic oscillations is first numerically investigated. Results demonstrate that for common soil, foundation and seismic excitation conditions, liquefaction leads to (a) significant reduction in dynamic stiffness and (b) increase in damping of the footing over pre-liquefied conditions. Based on these results, regression formulae for estimating static stiffness of surface footings on liquefied soil were developed. In the second part of the paper, parametric numerical analyses are presented for the typical case of bridge piers on liquefiable soil, with surface foundation and a remediated surface crust. Results from both harmonic steady-state and transient analyses indicate that the effect of soil liquefaction on the vibrational characteristics of the pier-foundation system decreases drastically with increasing soil crust thickness and, consequently, the intended natural base isolation of the structural system is mainly achieved by the reduction in free-field seismic ground response.

1. Introduction

Contrary to current design codes and guidelines, which dictate the use of deep foundations in soils prone to liquefaction, field observations from strong earthquakes [1, 2, 24] and a number of experimental studies [6, 12 – 14, 18, 32, 54] suggest the possibility of using shallow foundations on such soils, provided the existence of a competent surface layer to protect the superstructure from excessive settlement and/or post-shaking bearing capacity failure. Most recently, Bouckovalas et al [8] presented an integrated approach for Performance-Based Design (PBD) of shallow foundations on liquefiable soils with a non-liquefiable crust. The design is based on the idea of a natural or artificial crust, which needs not extend over the whole depth of the liquefiable sand, to take advantage of the observed benefits of settlement reduction and the seismic motion attenuation ("Natural Seismic Isolation – NSI") due to liquefaction of soil below the crust.

A key pre-requisite for the applicability of this new approach lies in the capacity to estimate the settlement of footings on liquefiable soil layers with a non-liquefiable crust. Naesgaard et al. [43] were pioneers in that direction, followed by Karamitros et al [26 – 28]. Both examined the case of a natural clay crust and used numerical analyses to correlate seismic settlements to the degraded factor of safety, at the end of seismic shaking while the subsoil is still liquefied, the first with the aid of design charts and the second by means of analytical relationships. Dimitriadi et al [15, 16] extended the work of Karamitros et al. [27] for the case of an artificial crust created by vibro-compaction of the native liquefiable soil, giving special emphasis on the required thickness and lateral extend of ground improvement. In parallel, Bray and Macedo [10] presented a simplified procedure for settlement computation in the case of an artificial soil crust with infinite lateral extend, based on regression analysis of results from 1300 nonlinear dynamic SFSI numerical analyses based on actual seismic excitation recordings. Compared to previous similar studies, Bray and Macedo also emphasized the effect on seismic settlements of volumetric-induced, and ejecta-induced ground deformation, which are commonly observed in the field but cannot be adequately captured by numerical analyses of continuous media.

Equally important for the seismic design of structures based on the new concept of *NSI*, is the simplified computation of the attenuated seismic motion at the free surface of liquefiable soil deposits. The available literature on this issue is even more limited than that for seismic settlements. Namely, Miwa and Ikeda [38] proposed to perform equivalent linear analysis, using strain independent values of elastic shear modulus for the liquefied soil layers approximately equal to 1-4% of the initial values without liquefaction. This methodology is

fairly simple but may under-predict spectral accelerations at the low structural period range, as it overlooks the well-established amplification effect during the pre-liquefaction part of the seismic excitation [62]. This effect is properly taken into account by two recently proposed methodologies, referenced in the literature as the "spectral envelope" [9] and the "spectral interpolation" [7] method. In both methodologies, the seismic ground response is computed twice, for liquefied and for initial non-liquefied soil conditions, and the results are combined to provide the target ground response. The required seismic response analyses can be performed with the widely known 1-D non-linear or equivalent linear methods, while their results are consequently interpreted using standard in-situ estimated factors of safety against liquefaction (FS_L) as the main variable.

Other recent studies on *NSI* include those by Sextos et al [50], Bouckovalas et al [8] and Vassilopoulou et al. [56] who presented a proof-of-concept study for three typical bridge systems, with approximately 90 m total span and 10 m pier height: a statically determinate concrete bridge, a statically indeterminate concrete bridge, and a steel overpass. Findings from these studies suggest that all three systems can tolerate the liquefaction-induced deformations without experiencing significant structural damage or loss of serviceability. Furthermore, compared to conventional pile foundation design, the new design concept led to 15-50% reduction in maximum bending moments on the pier and about 45-65% reduction in foundation cost, with the lowest reduction corresponding to the statically indeterminate concrete bridge.

In the context of the above research, a need arises to investigate the dynamic response of shallow foundations on liquefiable soils and its contribution to the overall structural system response. A rigorous treatment of dynamic stiffness and damping of footings on a liquefiable soil profile is a formidable problem due to the complexity and nonlinearity of the liquefaction phenomenon itself. Admittedly, despite extensive research on soil liquefaction over several decades, the mechanics of seismic wave propagation within liquefied soil remains poorly understood. It is known that shear-induced dilation under extremely low effective stresses leads to significant variation in excess pore pressure (and in ensuing seismic wave propagation velocity), even within the same loading cycle. As a result, the mechanical properties of liquefied soil are strongly time-variant during shaking, which renders the problem difficult to analyze. Additionally, the gradual pore pressure dissipation may induce considerable settlements and separation of the foundation from the ground in certain structural systems. An associated difficulty in handling the dynamic impedance problem stems from the need to consider a multilayer soil profile (i.e. at least three layers, including a non-liquefiable

surface layer, a middle liquefiable soil layer, and a non-liquefiable base stratum) with sharp impedance contrasts across the interfaces, which results in strong wave reflections and entrapment of seismic energy within the middle layer.

Most available solutions for the dynamic impedance of footings on non-liquefiable soil assume linear or equivalent-linear soil behavior and perfect contact between footing and soil [4, 19, 34, 37, 41, 44 – 45, 58 – 61]. Apart from convenience in application, the use of time-independent (though frequency-dependent) stiffness coefficients provides realistic means for developing simple engineering methodologies for the problem at hand. In the context of this simplified approach, soil-foundation interaction is represented by means of an equivalent spring-dashpot system connected to the footing, as shown in Fig. 1a. In the realm of standard elastodynamic theory, these formulations are often rigorous, as the stiffness and damping coefficients are obtained from exact numerical solutions of the corresponding boundary value problems [21].

The main scope of this paper is to investigate the dynamic stiffness and damping of rigid surface square footings resting on liquefiable soil under external harmonic loading. To this end, the fundamental case of a three-layer soil profile consisting of a liquefiable layer sandwiched between two stiff impermeable soil layers is considered. For the exploration of the problem, equivalent-linear elastic analyses are employed in conjunction with pertinent values for the material constants of liquefied soil. Recent experimental and analytical evidence suggest that during liquefaction, the shear wave propagation velocity can be reduced to 10 – 30% of its initial value [38, 53] while the soil material damping ratio may increase to over 20% [53], in agreement with a substantial increase in the imposed shear strains in the soil.

These observations allow for a simplification of the problem, which can be separated into two different phases: a) the initial phase [pre-liquefaction (*PL*)] and b) the phase during liquefaction [during-liquefaction (*DL*)] with the material properties of the liquefied soil adjusted over those prior to liquefaction. It is further assumed that the latter case starts from the beginning of shaking and that there is no sufficient soil permeability above and below the liquefied layer, so that the change in soil stiffness and damping due to liquefaction may be viewed as “permanent” during shaking. This is certainly a simplification, but can be considered realistic for the purposes of a dynamic earthquake analysis leading to easy-to-employ dimensionless charts and graphs regarding footing stiffness and damping. Through this decomposition and the aforementioned assumptions, one may analyze each phase separately by established elastodynamic theory.

This research concludes with parametric numerical studies of the seismic response of bridge piers on surface footings in liquefiable soil, modeled as described above. The aim of these proof-of-concept studies is to explore the relative effect on the superstructure response of two liquefaction-triggered, still independent response mechanisms: the attenuation of the seismic ground motion, briefly discussed in previous paragraphs, and the increase in superstructure-foundation vibration period, which will result from the decrease in soil impedances discussed herein. Results refer to both pre- and during-liquefaction cases, and are presented in frequency and time domain for bridge and footings accelerations by means of comparison graphs.

2. Methodology, Input Data and Assumptions

2.1 Problem Statement

The problem considered is depicted in Fig. 1.b: a massless rigid square ($B \times B$) surface footing resting on a liquefiable soil profile, subjected to external harmonic loading. A three-layer soil profile, including a surface clayey crust over a loose liquefiable sand layer followed again by a stiff clayey base, is assumed to this end. The dynamic impedance functions of the footing are numerically determined accounting for three oscillation modes (vertical, horizontal and rocking). The analyses refer to various footing sizes used for the foundation of both ordinary structures and bridge piers. Excitation frequencies cover the frequency range of importance in earthquake engineering. Having determined the associated dynamic impedance functions, one may investigate the impact of liquefaction on simple oscillators which can simulate a variety of actual bridge piers.

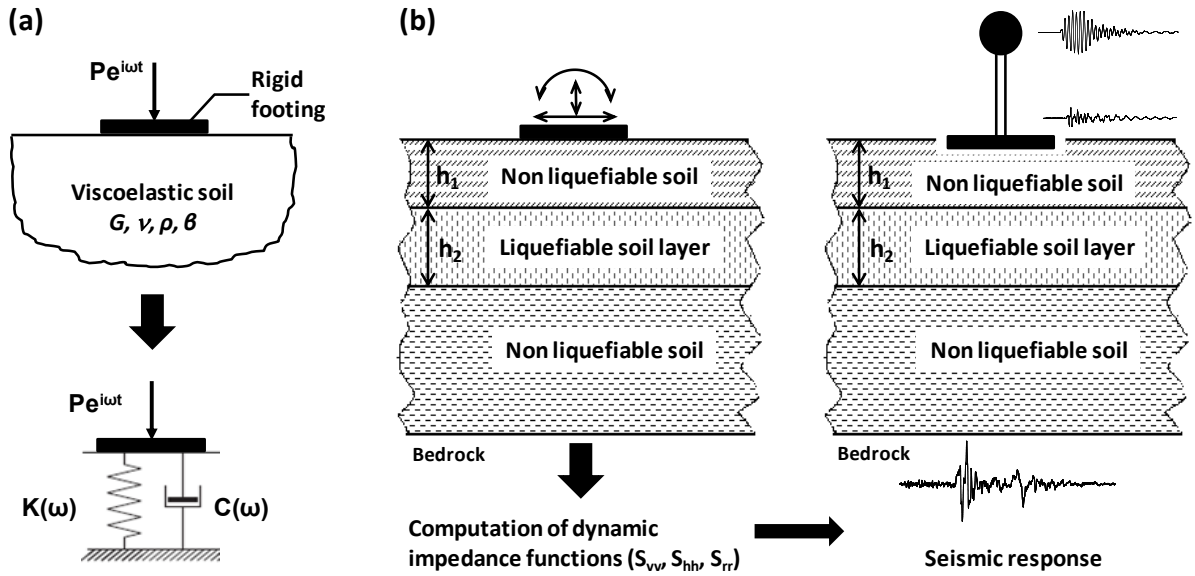

Fig. 1. a) Physical interpretation of dynamic stiffness via frequency dependent springs and dashpots, b) Problem under investigation

To examine the influence of liquefaction on the spring and dashpot coefficients, elastodynamic analyses were conducted for conditions prior to and during liquefaction. Of the few pertinent findings regarding the dynamic properties of liquefied soils, reference is made here to the work of Miwa and Ikeda [38], who propose to perform an equivalent linear analysis for the prediction of the seismic motion at the surface of the liquefied ground, using strain independent reduced values of elastic shear modulus for the liquefied soil layers. The key parameter for this kind of analyses is the shear wave velocity of the liquefied ground $V_{S,L}$, which was estimated by inverse analyses of actual recordings in liquefied sites and was consequently related to the factor of safety against liquefaction F_{SL} and the initial shear wave velocity without liquefaction $V_{S,o}$ (Table 1). The authors do not provide any details for the hysteretic damping ratio ξ_L of the liquefied soil that was used in their analyses. To fill this gap, one may refer to previous findings obtained from reverse analysis of relevant seismic recordings [36, 46], suggesting that the hysteretic damping ratio of liquefied sands is ξ_L = 20 - 30%, as well as to experimental data from cyclic triaxial tests [33] which indicate that it may rise to a maximum of ξ_L = 25 - 30% at double amplitude strain $\gamma_D \approx 1\%$ and eventually reduce to ξ_L = 10 - 20% at much larger strains.

Table 1. Proposed $V_{S,L}/V_{S,o}$ ratios by Miwa and Ikeda [38]

FS_L	0.3 - 0.6	0.6 - 0.9	0.9 - 1.0
$V_{S,L}/V_{S,o}$	0.10 - 0.14	0.12 - 0.16	0.14 - 0.19

To this end, it is assumed that during liquefaction the shear wave propagation velocity of the middle liquefiable soil is reduced to about 17% of its initial value, i.e. from V_{s2} = 150 m/s to V_{sliq} = 25 m/s. In view of the increase in energy loss due to material damping during liquefaction, in the present analyses material damping in the middle soil stratum is assumed to be β_2 = 3% prior to liquefaction and β_{liq} = 20% during liquefaction. Given the impermeable nature of the layers above and below the liquefied zone, no pore water pressure dissipation effects are considered during shaking. The soil below the surface layer is considered fully saturated, hence a uniform value for Poisson's ratio (ν = 0.49) is employed corresponding to a nearly incompressible medium.

Unless otherwise specified, the material properties of the surface layer employed in the analyses are shear wave propagation velocity V_{s1} = 100, 250 m/s, Poisson's ratio ν_1 = 0.33, material damping ratio β_1 = 3%, mass density ρ_1 = 2 Mg/m^3. The properties of the middle liquefiable layer are V_{s2} = 150 m/s, ν_2 = 0.49, β_2 = 3%, ρ_2 = 2 Mg/m^3 and the properties of the base stratum are V_{s3} = 300 m/s, ν_3 = 0.49, β_3 = 3%, ρ_3 = 2 Mg/m^3. With reference to the thicknesses of the surface crust and the liquefiable soil layer, three values are considered (h_1/B = 0.5, 1, 2 and h_2/B = 0.5, 1, 2). The total thickness of the soil profile is selected so that the presence of bedrock does not affect the dynamic response of the footing. Accordingly, the parametric investigation is focused upon the effect of thickness of the liquefied stratum, the thickness and stiffness of the non-liquefiable surface crust (which should meet the bearing capacity and settlement requirements of the superstructure under gravity loading [47]).

To obtain a set of governing problem parameters, standard dimensional analysis was employed. The problem involves six major dimensional independent parameters that have first-order influence on the response (M = 6). These are: thickness of surface crust, h_1, thickness of liquefiable layer, h_2, shear wave propagation velocity of non-liquefiable surface crust, V_{s1}, corresponding velocity of liquefiable layer, V_{s2}, footing width, B, and excitation frequency, f. Parameters such as the stiffness of the base layer and the total thickness of the soil profile have second order influence on the response and are not explored parametrically here.

In light of the two fundamental dimensions, length [L] and time [T] (N = 2) associated with the variables at hand, application of Buckingham's theorem [11] yields four dimensionless

groups ($M - N = 4$) controlling the response of the footing. These ratios were selected to be (h_1/B), (h_2/B), (V_{s1}/V_{s2}), ($\omega h_1/V_{s1}$), and are explored parametrically to assess their influence on the dynamic stiffness and damping of the footing.

2.2 Numerical methodology outline

It is briefly recalled that for static conditions, the stiffness of a rigid square or circular foundation is expressed in the following dimensionally consistent form [44]

$$\frac{K_{ij}^{0}}{G\,B^{m}} = f_{ij}\left(h_1/B, h_2/B, V_{s1}/V_{s2}, \omega h_1/V_{s1}, \nu\right) \tag{1}$$

where K^0_{ij} denotes the force or moment along the degree of freedom i of the footing for a unit displacement or rotation along the degree of freedom j. G denotes a pertinent soil shear modulus (typically that of the surface crust) and B the foundation width. The exponent m is equal to 1 for translational and 3 for rotational degrees of freedom. Finally, f_{ij} $(h_1/B, h_2/B, V_{s1}/V_{s2}, \omega h_1/V_{s1}, \nu)$ is a dimensionless factor dependent solely on the aforementioned dimensionless groups and the Poisson's ratio.

It is stressed that since this work deals with surface footings, the coupling term is negligible and only the vertical (K^0_{vv}), horizontal (K^0_{hh}) and rocking (K^0_{rr}) stiffnesses are considered.

For dynamic conditions, the dynamic impedance of the foundation is written in the familiar form

$$S_{ij}(\omega) = K_{ij}(\omega) + i\omega C_{ij}(\omega) \tag{2}$$

where K_{ij} and C_{ij} are the dynamic stiffness and damping coefficients, respectively, and i is the imaginary unit ($\sqrt{-1}$), which indicates a phase lag of 90° between the maximum dashpot force and the corresponding spring force during harmonic oscillations. Employing the familiar dimensionless frequency factor $a_0 = (\omega B/V_s)$, the dynamic impedance can be expressed as

$$S_{ij}\left(a_0\right) = K_{ij}^{0}\left[k_{ij}\left(a_0\right) + i\, a_0\, c_{ij}(a_0)\right] \tag{3}$$

where K^0_{ij} is the static stiffness and k_{ij}, c_{ij} are real-valued dimensionless stiffness and damping coefficients, respectively, which can be written as a function of dimensionless frequency a_0. It is noted that whereas k_{ij} may become negative at times (indicating a phase lag between excitation and response greater than 90°), c_{ij} is always positive so as to comply with thermodynamic constraints. It is worth mentioning that whilst parameter a_0 is essentially unique for half-space conditions (where B is the only parameter carrying units of length) it

might not be so in the presence of bedrock at a shallow depth [5], or in the presence of a significantly stiffer surface crust. For the interpretation of the results at hand, the alternative parameter ($\omega h_1/V_{s1}$) was selected [29].

2.3 Preliminary investigation using Cone Models

The dynamic impedance problem is first analyzed using Cone Model solutions. The most advanced version of this theory is due to Wolf and Deeks [61] who employed wave propagation in cones in conjunction with reflection and transmission coefficients at interfaces separating different soil layers, to develop a methodology for determining the dynamic stiffness and damping of surface or embedded cylindrical rigid foundations. Associated translational and rotational truncated cones (i.e., tapered beams and rods) are based on the convenient assumption of "plane sections remain plane" and the associated one-dimensional displacements. By means of these models, the complex three-dimensional elastodynamic problem is simplified to a problem of one-dimensional wave propagation, which admits closed-form solutions in homogeneous media, or in the form of infinite sums of transmitted and reflected waves in layered media. Apart from cylindrical foundations, various foundation shapes such as square footings of side B can be analyzed in an approximate manner, by considering an equivalent circular radius to match footing area for translational oscillation modes [$R = B/\sqrt{\pi}$], or pertinent moment of inertia for rotational oscillation modes [$R = B/4\sqrt{(3\pi)}$]. A multilayer soil profile overlying a half-space or bedrock may be readily employed, consisting of any number of horizontal layers. Dynamic stiffness and damping are evaluated for any single frequency under vertical, horizontal, rocking and torsional degrees of freedom. This convenient approach to foundation dynamics has been implemented in the computer code CONAN [61]. The accuracy of the model predictions has been verified in a number of studies, which suggest deviations in impedance functions from rigorous solutions in the range ± 20%, which are admissible from a geotechnical engineering viewpoint [23, 61].

2.4 Boundary-Element analysis

For verification purposes and to perform more accurate analyses of the problem at hand, a rigorous elastodynamic Boundary Element Method in three (3) dimensions was employed, implemented by means of the software platform ISoBEM [25]. BEM allows for the reduction in the dimensionality of the problem (from 3D to 2D), which means that only surfaces along boundaries need to be discretized. In these analyses, isoparametric four-noded linear quadrilateral elements are used for meshing the surfaces. Note that ISoBEM has been

successfully used to explore a variety of problems in soil and applied mechanics [22, 49, 55]. Three-dimensional models simulating a rigid square footing on a three-layer liquefiable soil in ISoBEM were set up with a dual purpose: a) to provide comparisons and b) to yield fitted formulae for static stiffness.

3. Parametric Analyses and Results based on Cone Solutions

3.1 Results for static stiffness

Fig. 2 presents results for the dimensionless static stiffness of a square rigid footing for both pre-liquefaction (V_{s1}/V_{s2}= 0.67 and 1.67) and during liquefaction (V_{s1}/V_{sliq}= 4 and 10) conditions. In the vertical axis, static stiffness K^0_{ij} is normalized with the shear modulus of the non-liquefiable surface crust ($G_1 = V_{s1}^2 \times \rho_1$) and the width of the footing (B) according to Eq. (1). Results are plotted against the thickness of the surface crust (h_1/B), for three values of the thickness parameter h_2/B (= 0.5, 1, 2).

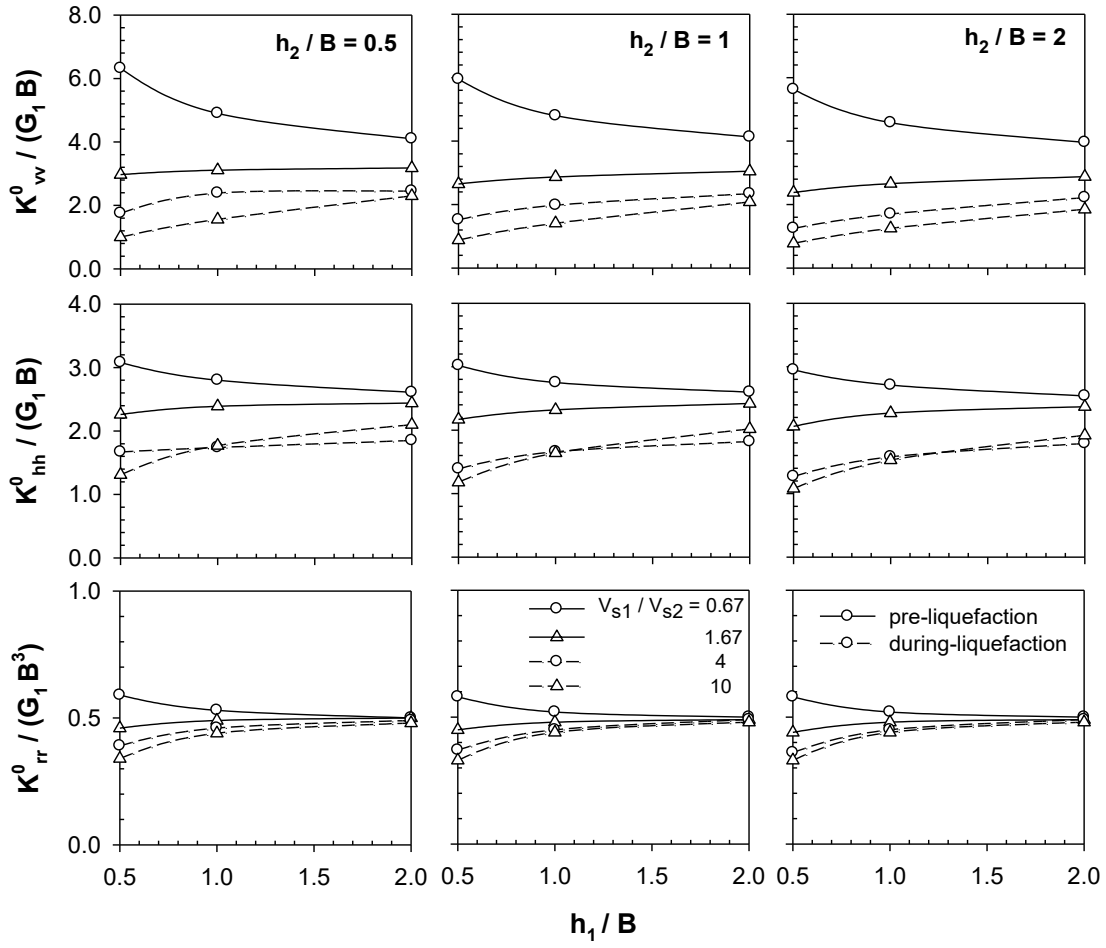

Fig. 2. Dimensionless static stiffness coefficients of square rigid footing on three-layer liquefiable soil based on cone method analyses.

The following noteworthy trends are evident in these graphs:

- The stiffness degradation of the liquefiable soil stratum during liquefaction associated with the increase in impedance contrast $\rho_1 V_{s1}/\rho_2 V_{s2}$ leads to a significant decrease in static stiffness, ranging from 28% to 78% for the vertical mode, 14% to 55% for the horizontal mode and 2% to 38% for the rocking mode. The highest decrease is observed for an initial shear wave velocity ratio $V_{s1}/V_{s2} = 0.67$.
- As the crust thickness ratio h_1/B increases, static stiffness for the liquefaction case increases, an anticipated trend given that for a thick surface layer the pressure bulb beneath the loaded area (about 1.5 B in diameter) does not extend to the soft liquefied soil.
- An increase in thickness of the liquefied soil (h_2/B) seems to further reduce the static stiffness coefficients, though this reduction is marginal for the range of parameters examined.

3.2 Results for dynamic impedance functions

With reference to the dynamic stiffness and damping, results are depicted in the form of the dimensionless ratios ($\tilde{K}_{ij} / K_{ij}$) and ($\tilde{C}_{ij} / C_{ij}$), as a function of the dimensionless frequency parameter ($\omega h_1 / V_{s1}$), Figs. 3–5. $\tilde{K}_{ij}$ and $\tilde{C}_{ij}$ denote the dynamic stiffness and damping during liquefaction, while K_{ij} and C_{ij} denote the corresponding pre-liquefied values. The specific normalization scheme along with the logarithmic scale for the horizontal axis allow for an insightful interpretation of the results.

Two distinct frequency regions, (I) and (II), are evident in Fig. 3. Region (I), defined for ($\omega h_1 / V_{s1}$) < 2, refers to footings having small to moderate width, B = 1 ~ 3 m, (h_1 is comparable to B), profiles with a soft soil crust, V_{s1} = 100 ~ 150 m/s, and low frequency excitation range f = 0 ~ 10 Hz. On the other hand, region (II) with ($\omega h_1 / V_{s1}$) > 2 corresponds to large footings, B > 4 m, profiles with a soft to moderate soil crust, V_{s1} = 100 ~ 250 m/s, and a high frequency excitation range f > 15 Hz. The same applies for the horizontal and rocking oscillation modes (Figs. 4 and 5), with the only difference being that the bound between these two regions for the horizontal mode is reduced to ($\omega h_1 / V_{s1}$) = 1. It is noteworthy that common buildings and structures fall into region (I). It is further observed that the dynamic stiffness is considerably reduced in region (I), while the corresponding dynamic damping ratio ($\tilde{C}_{ij} / C_{ij}$) increases well above unity. In region (II), dynamic stiffness starts to exhibit sharp undulations while ($\tilde{C}_{ij} / C_{ij}$) ratio tends to unity.

The following additional noteworthy trends are evident from Figs. 3–5:

- The variation in thickness of the surface crust has a significant effect on the dynamic stiffness and damping coefficients. Specifically, as the h_1/B ratio decreases dynamic stiffness decreases in region (I). In region (II), h_1/B ratio controls the undulations in impedance functions.
- With reference to damping, a significant increase during liquefaction is observed mainly due to the increase in material damping of the liquefied layer. Increase in the thickness of the surface crust results in amplification of damping for the vertical mode, while the opposite trend is noticed for the other two modes. Interestingly, the vertical damping coefficient ratio ($\tilde{C}_{vv} / C_{vv}$) exhibits a peak at around ($\omega h_1 / V_{s1}$) ≈ 0.75, which suggests development of a kind of "anti-resonance" at $T_{exc} \approx 2\ T_{s1}$ (i.e. $T_{s1} = 4h_1/V_{s1}$), possibly due to destructive wave interference during liquefaction. However, this behavior is not observed in the ($\tilde{K}_{vv} / K_{vv}$) ratio.
- The variation in thickness of the liquefiable soil stratum does not affect the dynamic stiffness of the footing, and the ($\tilde{K}_{ij} / K_{ij}$) curves almost coincide. On the contrary, h_2/B ratio seems to affect the damping ratio ($\tilde{C}_{ij} / C_{ij}$) which increases as h_2/B decreases, in both the horizontal and rocking mode.
- In Figs. 2c – 4c, it is noted that the initial shear wave velocity ratio V_{s1}/V_{s2} remains constant (= 2/3) while for the liquefied layer assumed V_{sliq} = 10, 25 and 35 m/s being ~ 7%, 17% and 23% of the initial shear wave velocity. Surprisingly, the V_{s1}/V_{sliq} ratio appears to affect only slightly the dynamic impedance functions.
- Regarding the vertical dynamic stiffness, it is noted that for some frequencies the ($\tilde{K}_{vv} / K_{vv}$) ratio admits negative values (with $\tilde{K}_{vv}$ being negative), which suggests a phase lag between excitation and response greater than 90°. Moreover, in the high frequency range and for h_1/B = 0.5, the dynamic stiffness coefficients are extremely high. The latter observation might indicate that the analysis provides unstable solutions at the high frequency range. This might lie partially on numerical instability due to the very low wave propagation velocity in the sand layer.

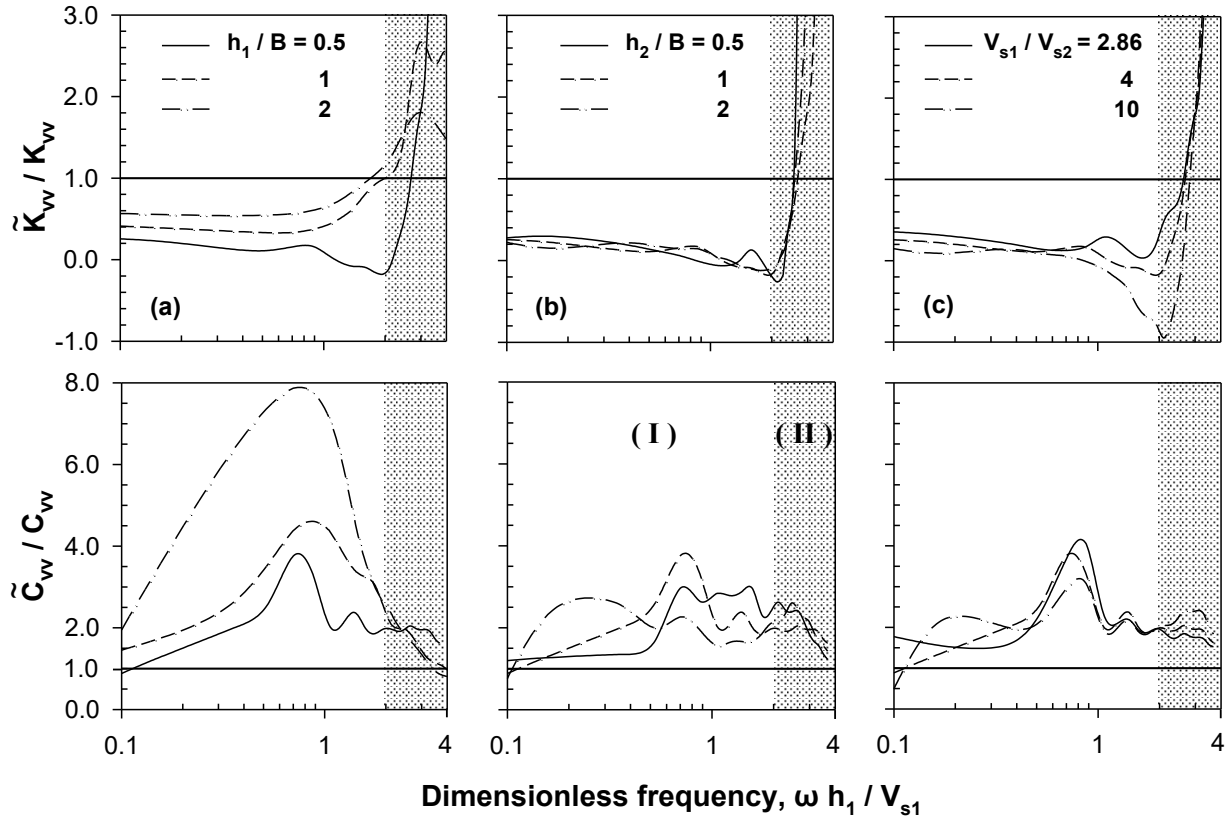

Fig. 3. Vertical dynamic impedance coefficients during liquefaction of square footing normalized with the corresponding pre-liquefied impedance coefficients; Effect of a) thickness of surface crust, b) thickness of liquefiable soil layer, c) shear wave velocity ratio; $h_1/B = 0.5$, $h_2/B = 1$, $V_{s1}/V_{s2} = 2/3$ (4).

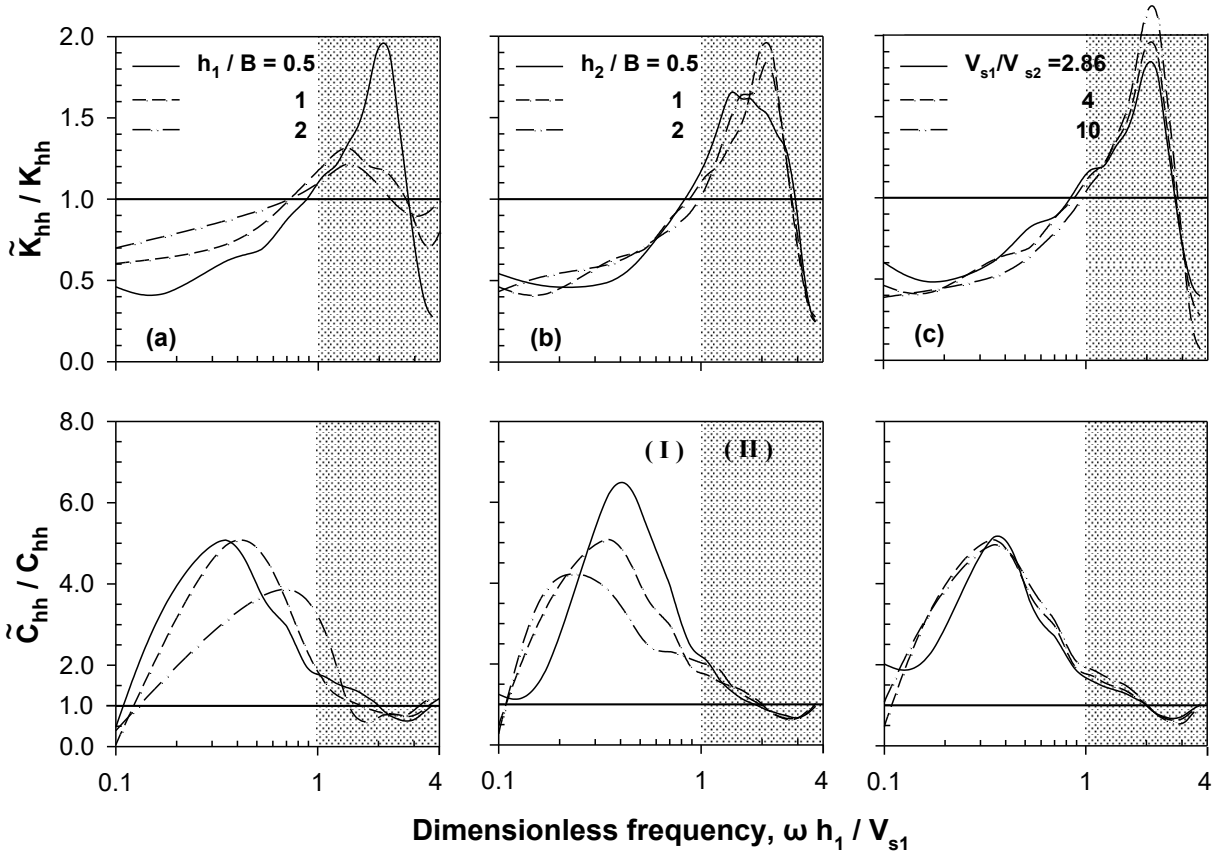

Fig. 4. Horizontal dynamic impedance coefficients during liquefaction of square footing normalized with the corresponding pre-liquefied impedance coefficients; Effect of a) thickness of surface crust, b) thickness of liquefiable soil layer, c) shear wave velocity ratio; $h_1/B = 0.5$, $h_2/B = 1$, $V_{s1}/V_{s2} = 2/3$ (4).

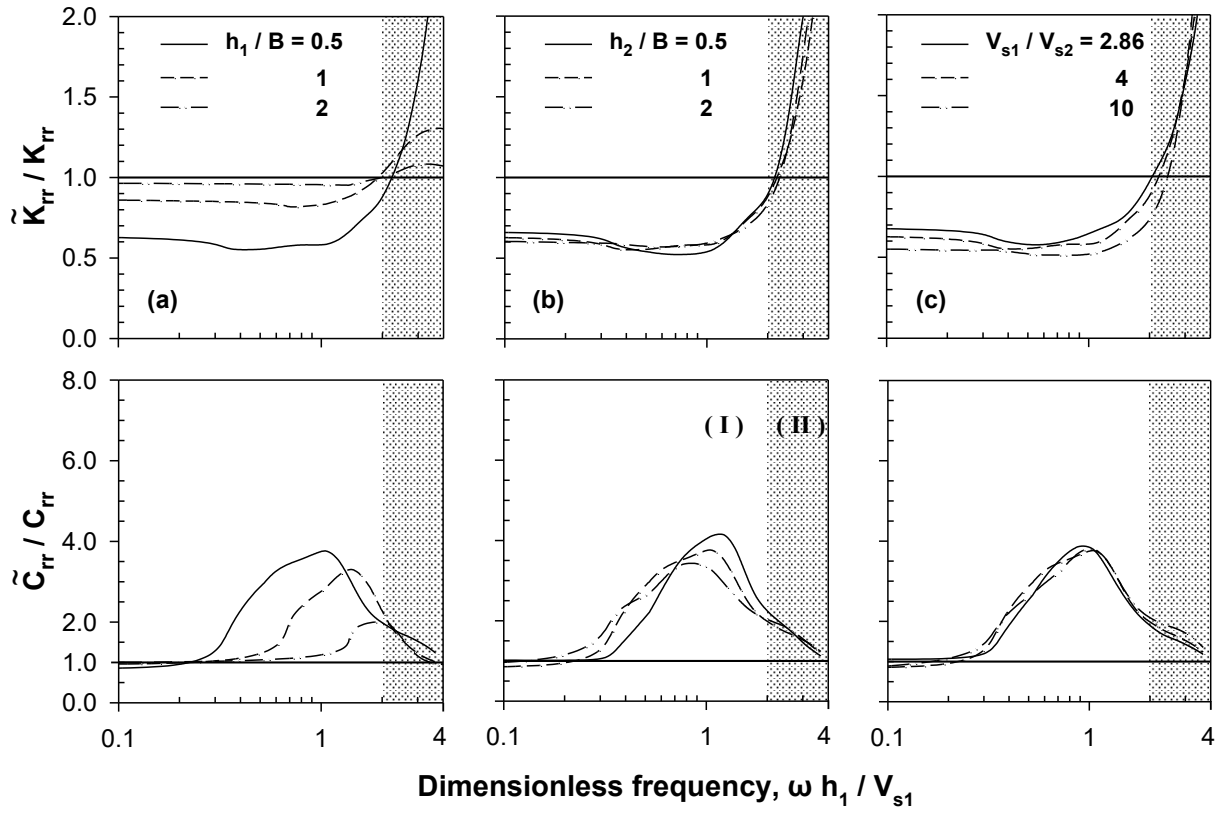

Fig. 5. Rocking dynamic impedance coefficients during liquefaction of square footing normalized with the corresponding pre-liquefied impedance coefficients; Effect of a) thickness of surface crust, b) thickness of liquefiable soil layer, c) shear wave velocity ratio; $h_1/B = 0.5$, $h_2/B = 1$, $V_{s1}/V_{s2} = 2/3$ (4).

4. Parametric Analyses and Results based on Boundary-Element Solutions

4.1 Check accuracy of BEM analyses

In the realm of the BEM formulation, convergence studies for foundation impedance and dynamic soil-structure interaction problems have been conducted by several researchers [3,4]. The most significant factors in providing accurate solutions are the distance of the non-reflecting truncation boundary and the boundary element size [52]. To select the optimum model, various 3D configurations (half and quarter domain) and mesh sizes for each oscillation mode were examined.

Taking advantage of the symmetry of geometry and loading, for the vertical (symmetric) oscillation mode, only one quarter of the system needs to be analyzed. For the horizontal and rocking (antisymmetric) modes, analyzing a half model provides more accurate results. To this end, the footing surface and the region around the footing up to a distance $3B$ is

discretized using iso-parametric four-noded quadrilateral linear elements with element length about 1/12 of the shear wavelength. Moreover, the surface beyond this region and up to a distance of 5*B* requires a fine mesh (element length = 1/8 of shear wavelength). The same also applies for the interface between first and second layer. In addition, discretization of the ground surface and the interfaces up to a distance of at least 10*B* to 15*B* beyond the edge of the foundation is necessary for obtaining accurate results. Coarser elements with lengths of 1/3 to 1/2 of the shear wavelength are adequate for distant points [4].

For the vertical and horizontal oscillation modes, a uniform unit vertical and horizontal displacement, respectively, is applied to all element nodes of the footing and the resulting load is computed from the tractions developed on the element nodes [29]. For the rocking mode, a unit rotation is applied.

Because of lack of solutions for stiffness of square footings on three-layer soil profiles, the solution was checked by a) applying to all soil layers the same properties to obtain the stiffness of a rigid square footing on a half-space, and b) applying to the second and third layer the same properties, forming a two-layer soil profile, and comparing the results for stiffness with results in literature.

To verify the BEM model, comparative studies are conducted with published results. Table 2 provides the comparison of ISoBEM results for normalized static stiffness of rigid square footing on half-space, for all three oscillation modes, with the empirical formulas from Pais and Kausel [45]. In Table 3, results for the horizontal static stiffness of a two-layer soil profile ($v_1 = v_2 = 0.4$) are compared against corresponding solution obtained from Ahmad and Rupani [4]. Fig. 6 depicts the comparison of ISoBEM results for horizontal, vertical and rocking impedance of a square footing resting on a uniform soil layer over a half-space ($V_{s1}/V_{s2} = 0.8$, $H/(B/2) = 1$, $v_1 = v_2 = 0.33$, $\rho_2/\rho_1 = 1.13$, $\beta_1 = 0.05$, $\beta_2 = 0.03$) with those reported by Wong and Luco [59]. Evidently, results obtained by analyzing the developed model in ISoBEM are in reasonable agreement with the published results.

Table 2: Comparison of normalized static stiffness $K^0_{ij}/(GB^m/2)$ of a rigid square footing on half-space.

	$K^0_{ij}/(GB^m/2)$		
Oscillation mode	[Reference 45]	ISoBEM	Diff. (%)
Vertical (m=1)	7.12	6.93	2.7
Horizontal (m=1)	5.75	5.64	1.9
Rocking (m=3)	6.67	6.92	-3.7

Table 3: Comparison of normalized horizontal static stiffness $K^0_{hh}/(G_1B/2)$ of a rigid square footing on a two-layer soil profile.

H/B/2	$K^0_{hh}/(G_1B/2)$					
	$V_{s1}/V_{s2} = 0.5$			$V_{s1}/V_{s2} = 2$		
	ISoBEM	Reference [4]	Diff. (%)	ISoBEM	Reference [4]	Diff. (%)
1	7.73	7.9	-2.2	3.79	3.8	-0.3
2	6.75	6.8	-0.7	4.50	4.4	2.2
4	6.22	6.2	0.3	5.09	5.0	1.8

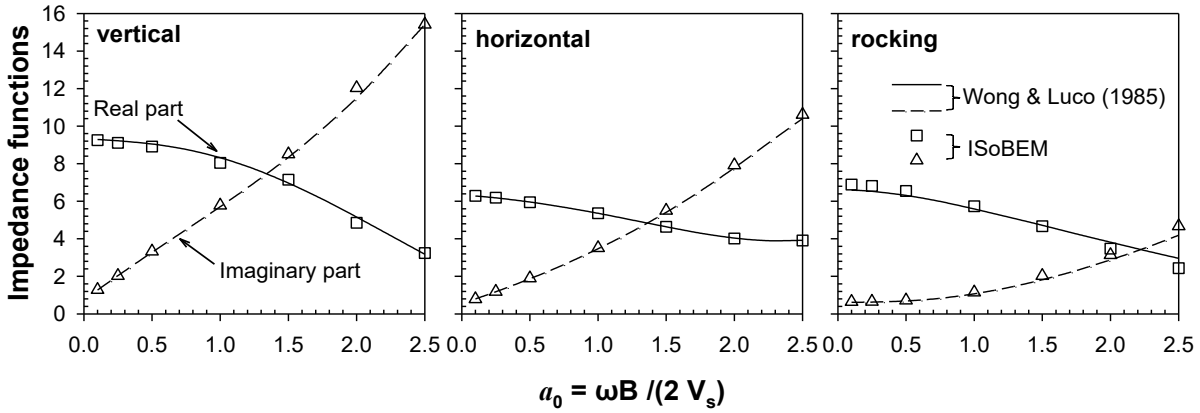

Fig. 6. Comparison of dynamic impedance functions of a square footing resting on a two-layer soil profile.

4.2 Results and regression formulae for static stiffness

Results for the dimensionless static stiffness during liquefaction ($\tilde{K}^0_{ij}$ /K^0_{ij}), obtained by means of ISoBEM, for all three degrees of freedom, are presented in Table 4. The outcome of this analysis demonstrates a significant loss of footing stiffness during liquefaction, being in meaningful agreement with the preliminary results using cones. In the context of these analyses, it is worth mentioning that:

- The decrease in static stiffness ranges from 11% to 84% for the vertical mode, 11% to 56% for the horizontal mode and 1% to 59% for the rocking mode, being comparable to those predicted from the cone analyses.
- The highest decrease understandably occurs when a very thin surface clay crust (h_1/B = 0.5) overlies a thick liquefiable sandy layer (h_2/B = 2), while the lowest decrease is

observed in the opposite case, where a thin liquefiable sandy layer (h_2/B = 0.5) underlies a thick surface clay zone (h_1/B = 2).

- It is observed that for a given set of (h_1/B) and (h_2/B) ratios the percentage of decrease in stiffness is independent of (V_{s1}/V_{sliq}), which is not obvious in the preliminary results.
- With reference to the horizontal mode, it is noted that the thickness of the liquefiable layer (h_2/B) appears to not affect considerably the horizontal stiffness.
- Regarding rocking response, BEM results reveal a significant reduction in static stiffness, especially for h_1/B = 0.5. On the contrary, for h_1/B = 2 the reduction is negligible.

Table 4: Static stiffness coefficients during liquefaction of square footing normalized with the corresponding pre-liquefaction static coefficients.

		$\tilde{K}^0_{ij}/K^0_{ij}$								
		Vertical			Horizontal			Rocking		
		V_{s1}/V_{sliq}								
h_1/B	h_2/B	4	7	10	4	7	10	4	7	10
0.5	0.5	0.41	0.38	0.39	0.54	0.52	0.54	0.53	0.53	0.55
	1	0.25	0.24	0.26	0.48	0.48	0.52	0.46	0.45	0.48
	2	0.17	0.16	0.17	0.44	0.45	0.50	0.42	0.41	0.44
1	0.5	0.68	0.64	0.64	0.74	0.70	0.71	0.88	0.87	0.88
	1	0.51	0.47	0.47	0.69	0.66	0.69	0.85	0.83	0.85
	2	0.36	0.32	0.33	0.64	0.63	0.67	0.81	0.82	0.82
2	0.5	0.89	0.87	0.87	0.89	0.86	0.86	0.99	0.99	0.99
	1	0.80	0.77	0.76	0.85	0.83	0.84	0.97	0.97	0.97
	2	0.68	0.63	0.63	0.81	0.81	0.83	0.96	0.97	0.99

Fig. 7 depicts the variation of normalized static footing stiffness in the post-liquefaction case with the thickness of the improved surface crust (h_1/B), for three values of the liquefied soil zone, (h_2/B). Using non-linear regression analysis based on the results of Fig. 7, a set of predictive equations was derived, which is provided in Appendix A. These relations, although complex, can be used in applications for a preliminary assessment of the problem. Note that the regression formulae are valid for during-liquefaction conditions, i.e. for (V_{s1}/V_{sliq}) > 1, and for the parameter range 0.5 ≤ (h_2/B) ≤ 2.0. Numerical values obtained from the regression formulae are illustrated in Fig. 7.

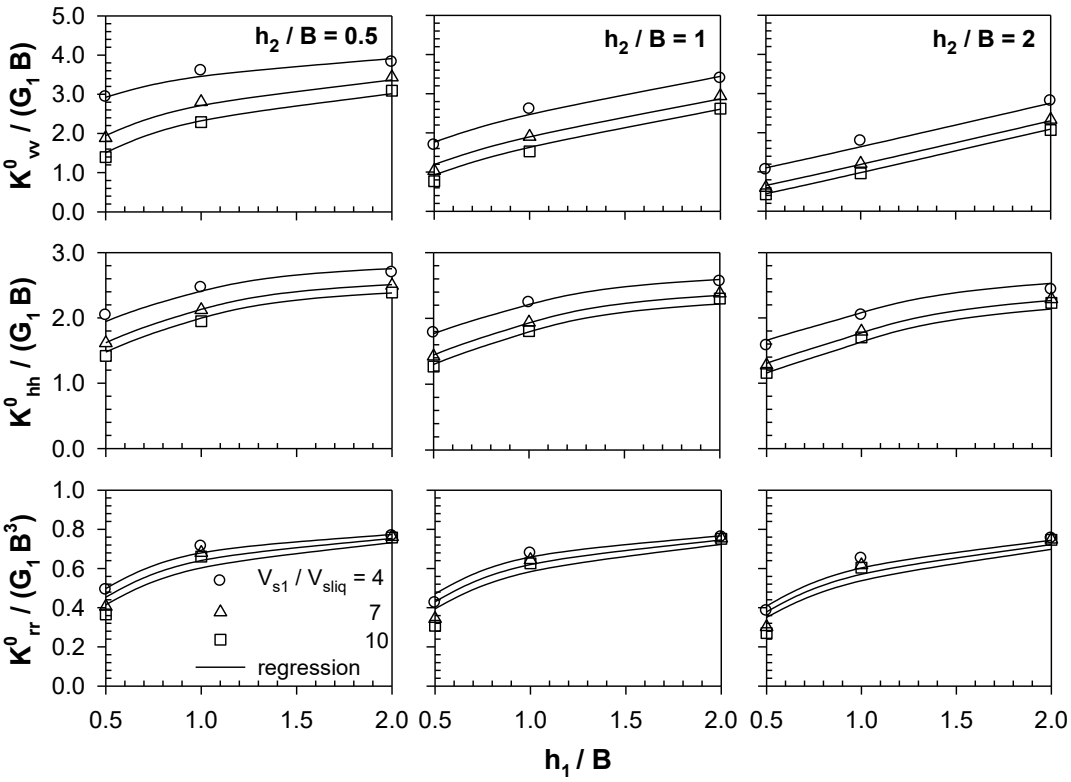

Fig. 7. Normalized static stiffness of square rigid footing on liquefied soil based on BEM results and results obtained using regression formulae.

4.3 Comparison of cone and BEM solutions

Results obtained from the cone solution were found to be in meaningful agreement with those obtained by the boundary element method. For horizontal oscillations, the comparisons are summarized in Table 5. It is observed that BEM typically predicts higher values for static stiffness. The maximum discrepancies are on the order of 20%, and are anticipated in light of the complexity of the problem and the extremely low value of shear wave velocity considered for the liquefied stratum (V_{sliq} = 25 m/s). Also, the low value of the shear wave velocity of the crust seems to play an important role in these deviations. The same also holds for the other two modes of oscillation [30, 31].

Regardless of the observed discrepancies in absolute stiffnesses, the reduction in static stiffness triggered by liquefaction is comparable in the two approaches, as shown in Section 3.1. Hence, rigorous elastodynamic boundary element results confirm the significant loss of stiffness of the foundation during liquefaction. From a geotechnical engineering viewpoint, results are generally comparable and the results from CONAN analyses can be used for a preliminary assessment of the effect of liquefaction on the stiffness of the footing in an equivalent-linear sense.

Table 5: Comparison of horizontal static stiffness coefficients (BEM vs Conan)

		$K^0_{hh\ (BEM)} / K^0_{hh\ (Cone)}$			
		V_{s1} / V_{s2}			
h_1/B	h_2/B	0.67	1.67	4	10
0.5	0.5	1.24	1.16	1.22	1.08
	1	1.22	1.13	1.28	1.08
	2	1.21	1.12	1.24	1.07
1	0.5	1.19	1.15	1.41	1.10
	1	1.19	1.14	1.35	1.10
	2	1.18	1.11	1.29	1.11
2	0.5	1.16	1.14	1.45	1.14
	1	1.16	1.13	1.41	1.14
	2	1.18	1.13	1.36	1.16

Fig. 8 depicts a comparison between dynamic stiffness and damping coefficients obtained by means of Cone and BEM solutions. The case where (h_1/B) = 1, (h_2/B) = 1 and (V_{s1}/V_{sliq}) = 4 is illustrated. Spring coefficient $\tilde{k}_{ij}$ and dashpot coefficient $\tilde{c}_{ij}$ are plotted, in accordance with Eq. 3, against the dimensionless frequency coefficient a_0 (= $\omega R/V_{s1}$) with $R = B/\sqrt{\pi}$ being the equivalent circular radius stemming from the cone solution, and $\omega(B/2)/V_{s1}$ for results obtained using the boundary element method. For simplicity, the same equivalent radius was also used for the rocking mode. The agreement between Cone model and BEM predictions is satisfactory. Similar good agreement (not shown) was observed with other cases.

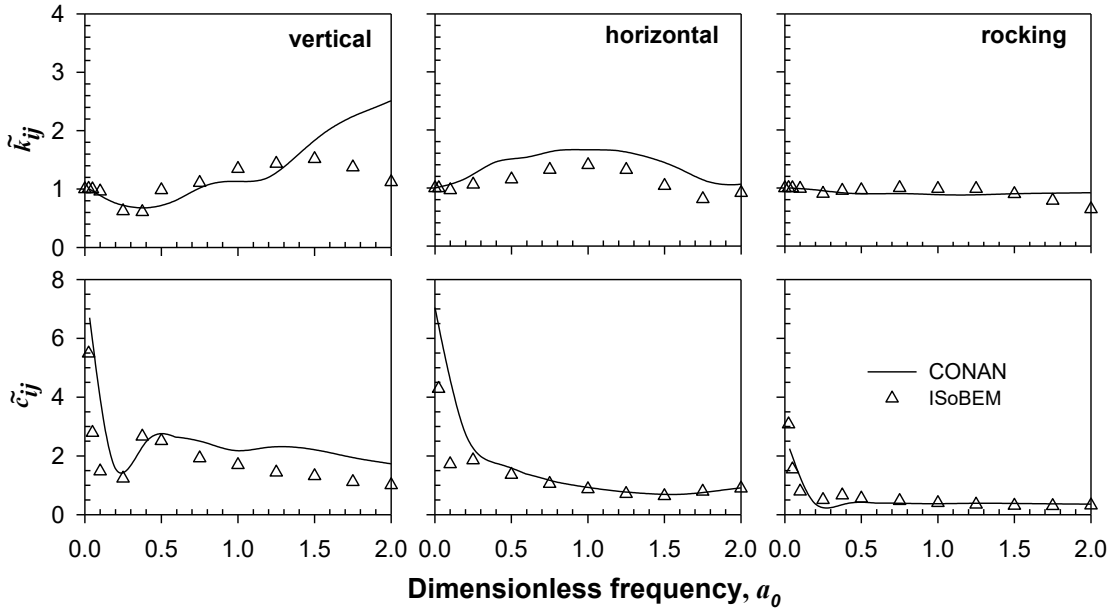

Fig. 8. Comparison between Cone model and BEM results for dynamic stiffness and damping coefficients; h_1/B = 1, h_2/B = 1, V_{s1}/V_{sliq} = 4.

5. Parametric investigation of the seismic response of bridge piers

The structural system examined is illustrated in Fig. 9a and may be considered as an idealized model of an actual bridge. The pier is of single-column type with diameter d = 1.3 m, founded on a spread footing resting on soil prone to earthquake liquefaction. The axial gravity load accommodated by the system is 3500 kN, typical of a two lane highway bridge with spans of about 35 m. The bridge deck is free to rotate. Two column heights are considered, H_c = 5 and 10 m, to explore the influence of the proposed geotechnical isolation method to both squat-like and slender-like structural elements. It is also assumed that the shape of the spread footing is square of side B = 7 m while its mass is equal to 120 Mg, which is a reasonable value for a large foundation. For simplicity and to be comparable with the results for the dynamic impedance functions obtained in Sections 3 and 4, it is further assumed that the foundation has no embedment and, thus, there is no kinematic effect. The analysis is carried out using the modified version of the numerical code SFIAB developed by the authors [40].

The properties of the liquefiable soil profile are given in Fig. 9a. Two values for the thickness of the improved non-liquefiable surface crust, h_1 = 3.5 and 7 m, and two values for the shear wave propagation velocity, V_{s1} = 100 and 250 m/s, are examined. Note that the depth setting the rigid bedrock is assumed to be either 20 m or about 110 m, conforming to a shallow and a deep profile, respectively. It should be mentioned that before one can rely on the proposed approach there also needs to check whether the strength and the thickness of the crust below the foundation is such that there will not be a punching failure of the foundation through to the liquefied layer below, such as discussed by a number of papers ([8, 15, 16, & 28]) cited early in the manuscript.

The soil-foundation-pier system is excited by vertically propagating S-waves corresponding to a horizontal rock outcrop motion. Both frequency- and time-domain analyses were conducted to investigate the impact of liquefaction on: a) the vibrational characteristics (i.e., fundamental period, overall damping) of the foundation-bridge pier system, and b) the response of the system to recorded earthquake motions. In time-domain analyses, the Pacoima (Northridge 1994 earthquake) excitation time history having a Peak Ground Acceleration (PGA) of 0.42g is used. The acceleration time history and the 5 and 10% damped acceleration response spectra are shown in Fig. 9b.

Owing to the common practice by structural engineers to adopt static foundation stiffness for design purposes, it was deemed useful to explore the possibility of using only the static

value of foundation stiffness, instead of the actual frequency-dependent stiffness, for determining the bridge response.

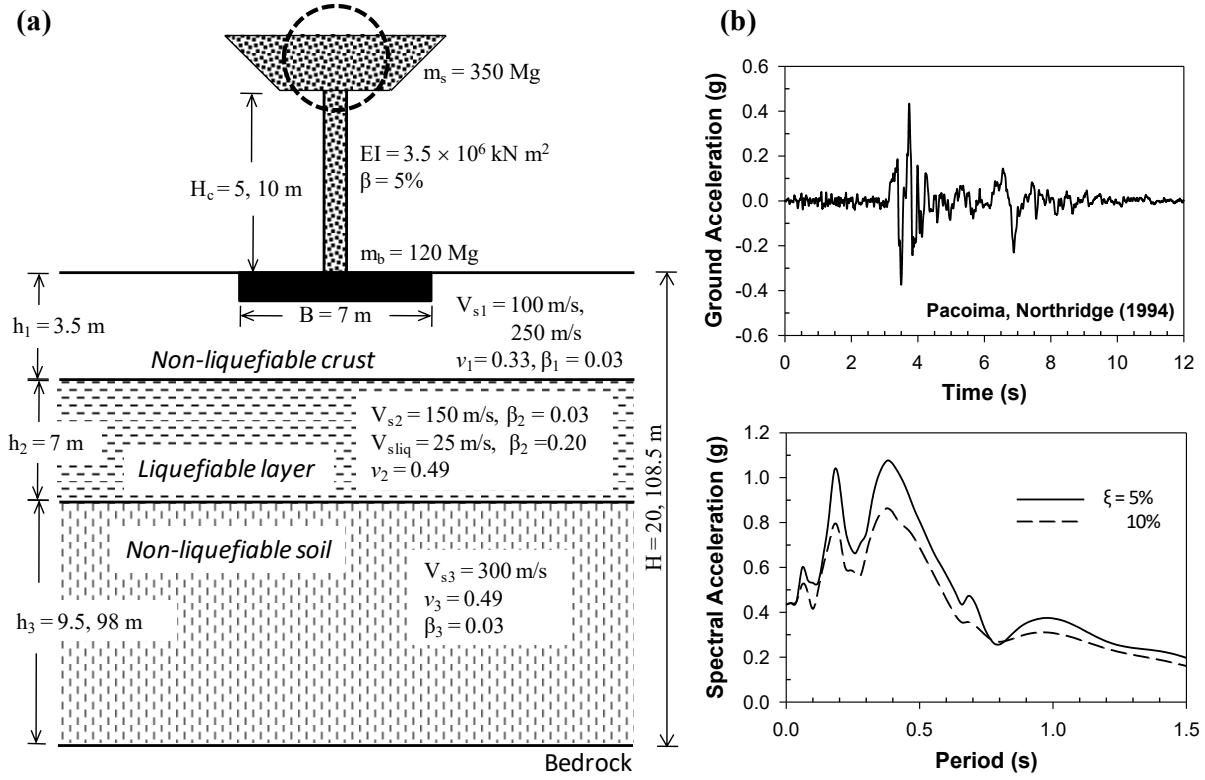

Fig. 9. a) Bridge pier supported on a spread footing on liquefiable soil with improved non-liquefiable surface crust. b) Acceleration time history and 5, 10% damped spectra.

5.1.Application to short bridge piers on a deep soil profile

The harmonic steady-state and transient seismic response of a short pier, H_c = 5 m, with a "soft" improved surface zone (V_{s1} = 100 m/s) prior to the onset and during the course of liquefaction, resting on a deep soil profile (h_3 = 98 m), are depicted in Figs. 10 and 11. The following noteworthy observations can be made with the help of these graphs:

- For the pre-liquefaction case, the fundamental natural period, T_1, of the soil deposit appears to be 1.46 s, which is close to the natural period of the thick and stiff base stratum (i.e., $4h_3 / V_{s3}$ = 4×98/300 ≅ 1.31 s). The second natural period, T_2, of the soil deposit is 0.49 s, which is approximately 1/3 of the fundamental period T_1 – as anticipated for a shear system. The fundamental period of the pier-foundation-soil system is equal to $\tilde{T}$ = 0.54 s – which is close to the second resonance of soil – and seems to be crucial to the response of the pier. The amplitude of pier response is about A = 11.3, corresponding to about 4.4 % [A ≅ $1/(2\tilde{\beta})$] of

overall damping of the pier-foundation-soil system, which seems reasonable if one considers that the hysteretic material damping is 3%.

- For the liquefaction case, the harmonic steady-state transfer functions display two peaks, at 1.78 s and 1.2 s. The first resonance in the soil occurs at 1.78 s and the second one at 1.2 s exhibiting a marginally greater amplification. The second peak can be associated with resonance of the liquefiable layer (i.e., $4h_2 / V_{sliq} = 4 \times 7/25 \cong 1.12$ s). The fundamental period of the pier-foundation-soil system, $\tilde{T} = 0.61$ s, lies very close to the third-mode resonance occurring at 0.59 s. The amplification factor for the bridge pier is about $A = 4.74$ and implies that the effective damping of the overall system reaches up to 10.5% – mainly due to damping in the liquefied layer. Finally, the maximum amplification in the soil is about two times smaller compared to that in pre-liquefaction conditions.

- The increase in the fundamental period of the soil can be verified by means of a simple analytical solution. Using the Rayleigh quotient along with a pertinent shape function obtained from the lateral equilibrium of a soil column having the same layering and inhomogeneity properties [42], a generalized closed-form solution is developed for the prediction of the fundamental natural period of a three-layer soil deposit (Appendix B). The analytical solution for pre- and during liquefaction conditions yields $T_1 = 1.44$s and 1.64s, respectively, which are very close to the numerically evaluated ones.

- Comparison of amplification functions reveals two important features of the liquefaction effect on seismic response of the superstructure: a) the fundamental oscillation period increases from $\tilde{T} = 0.54$ s to $\tilde{T} = 0.61$ s, a shift of about 11.5%, and b) the amplitude of the response decreases considerably by 58%. For pre-liquefaction conditions, the well-known formula of Veletsos and Meek [57] yields,

$$\tilde{T}_{pre} = T_{st}\sqrt{1+\frac{K_{st}}{K_{hh}^{0}}\left(1+\frac{K_{hh}^{0}H_c^2}{K_{rr}^{0}}\right)} = 0.41s\sqrt{1+\frac{8.41\cdot10^4}{4.23\cdot10^5}\left(1+\frac{4.23\cdot10^5\cdot5^2}{3.97\cdot10^6}\right)} = 0.54\ s \tag{4}$$

Likewise, during liquefaction conditions,

$$\tilde{T}_{liq} = 0.41s\sqrt{1+\frac{8.41\cdot10^4}{1.95\cdot10^5}\left(1+\frac{1.95\cdot10^5\cdot5^2}{2.55\cdot10^6}\right)} = 0.62\ s \tag{5}$$

where T_{st} is the fixed-base fundamental period of the superstructure $T_{st} = 2\pi\,[m_s / (3EI/H_c^3)]^{1/2} = 0.41$ s (Fig. 10).

Evidently, the fundamental period of pier-foundation-soil system $\tilde{T}$ for both pre- and during-liquefaction is quite close to the fixed-base fundamental period of the structure. This

can be attributed to the compliance of the deck, which is free to rotate at the top and, thus, the response is controlled to a greater extent by the characteristics of the superstructure. Moreover, the dominant periods of the rock-outcrop motion are within the range 0.15 to 0.5 s, which also plays an important role in the response.

In the time domain (Fig. 11), comparison of acceleration histories shows a remarkable de-amplification of the seismic motion during liquefaction which has a beneficial effect on the seismic response of the pier.

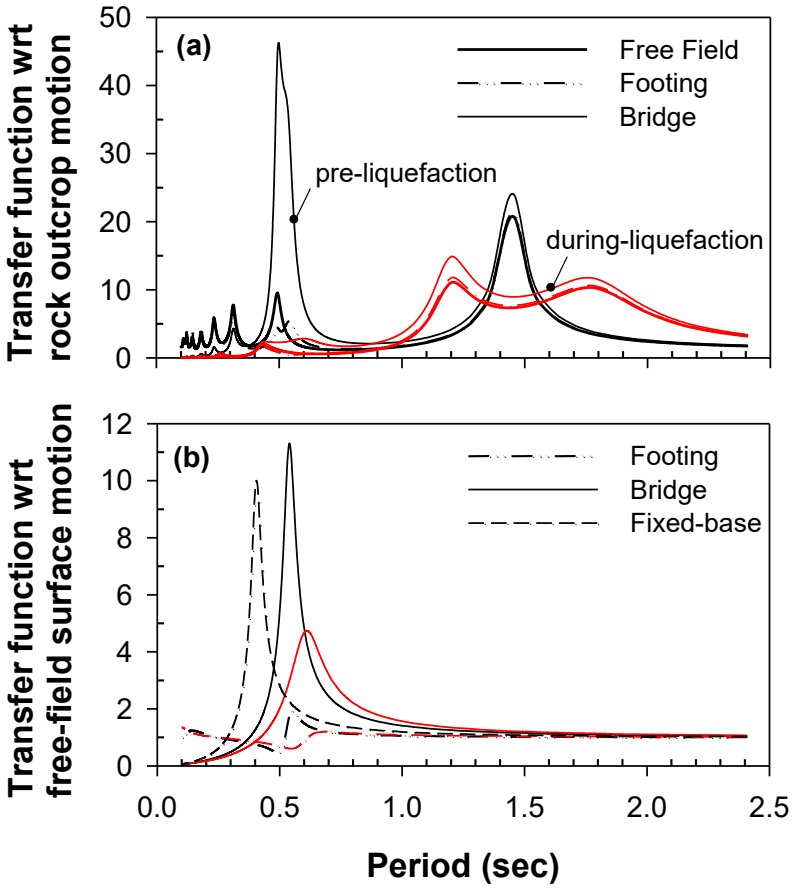

Fig. 10. Harmonic steady-state transfer functions for pre- and during-liquefaction for a short bridge pier; H_c = 5 m, B = 7 m, h_1 /B = 0.5, h_2 /B = 1, V_{s1} /V_{s2} = 2/3 (4).

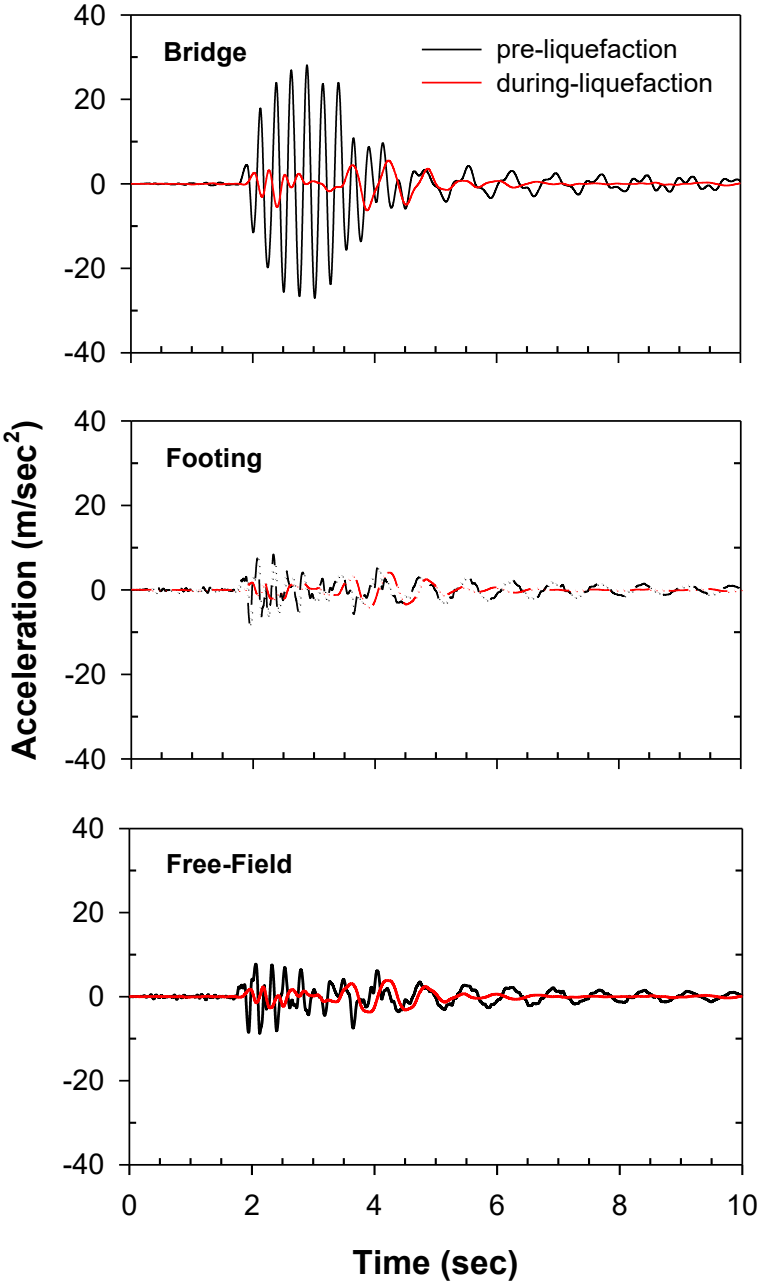

Fig. 11. Comparison of acceleration histories in pre- and during-liquefaction conditions for a short bridge pier; H_c = 5 m, B = 7 m, h_1 /B = 0.5, h_2 /B = 1, V_{s1} /V_{s2} = 2/3 (4).

5.2 Application to tall bridge piers

Results presented in this section refer to a bridge pier with height twice as large as in the previous case (H_c = 10 m). The following noteworthy observations can be made:

- For pre-liquefaction conditions, the fundamental period of the pier-foundation-soil system is $\tilde{T}$ = 1.32 s, which is close to the first resonance of the soil layer, and the amplification factor is equal to A ≅ 10.6, as shown in Fig. 12a. For liquefaction conditions,

the fundamental period shifts to $\tilde{T}$ = 1.41 s and the amplification factor drops to A ≅ 8.9. Evidently, the period shift is smaller compared to that for the short pier (an increase of about 6.4%) and the decrease in amplitude is about 16%.

- The minor effect of liquefaction on the seismic response of the pier is apparent in Fig. 12b. This is anticipated in light of the response spectrum of the rock outcrop motion (Fig. 9b). Indeed, both fundamental periods for pre- and during-liquefaction conditions, 1.32 and 1.41s, are far beyond the range of predominant periods of the excitation, which indicates that an increase in natural period due to liquefaction has little impact on the pier response.
- Additionally, Fig.12 shows the transfer function and bridge acceleration history of the fixed-base pier – a common assumption of designers – to highlight the role of geotechnical engineering in the seismic vulnerability assessment of structures.

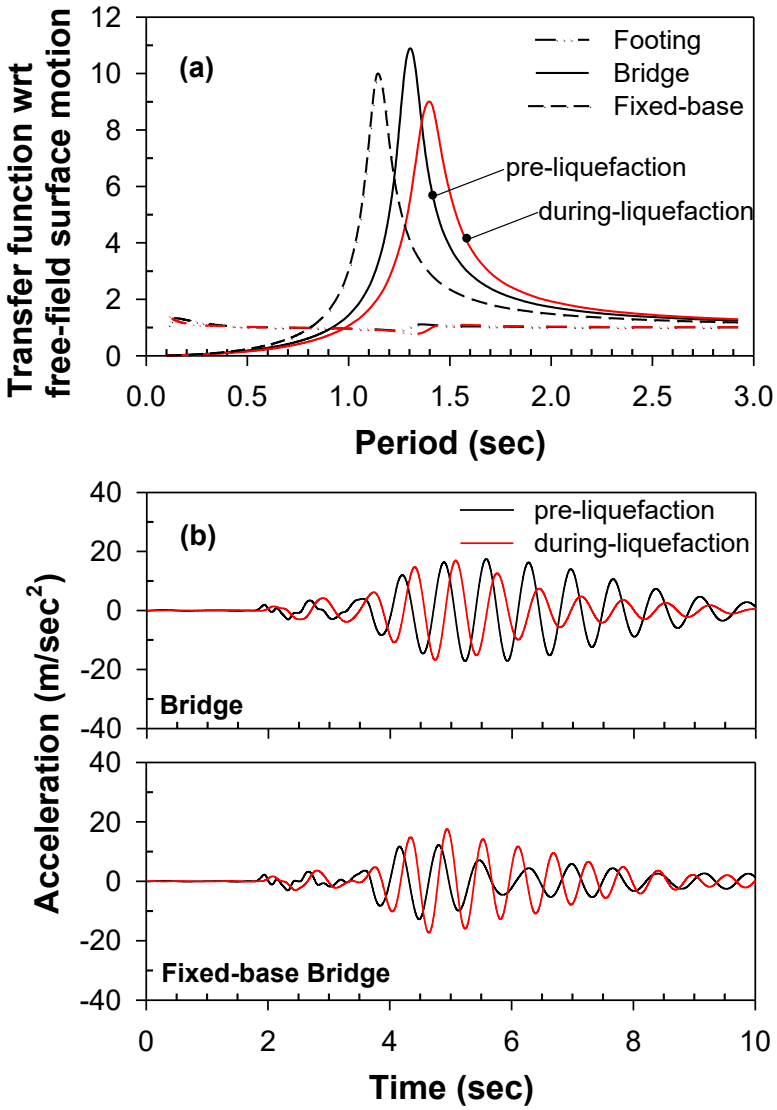

Fig. 12. Comparison of a) harmonic steady-state transfer functions and b) bridge acceleration history in pre- and during-liquefaction conditions; H_c = 10 m, B = 7 m, h_1 /B = 0.5, h_2 /B = 1, V_{s1} /V_{s2} = 2/3 (4).

5.3 Influence of stiffness of the non-liquefiable surface crust

To elucidate the role of the surface crust on bridge response, a stiffer surface zone with shear wave propagation velocity V_{s1} = 250 m/s is considered. The analysis refers to the short pier (H_c = 5m). Important findings from Fig. 13 are summarized below:

- The stiffness of the thin surface soil layer does not alter substantially the free-field response. Likewise, the fundamental period of the soil deposit is almost invariant in the pre- and during-liquefaction case. However, the increase in stiffness of the surface layer does modify the fundamental period of the pier at $\tilde{T}$ = 0.43 s and 0.45 s for pre- and during-

liquefaction case, respectively, bringing it closer to the fixed-base fundamental period, i.e., T_{st} = 0.41 s. This indicates that the stiff surface soil layer operates essentially as a fixity condition for the superstructure, thus cancelling out any SFSI effect of the underlying liquefiable soil layer.

- With reference to response amplitude, for no liquefaction conditions the amplification factor A is about 9.9, leading to a damping ratio almost identical to that of the superstructure. For conditions during liquefaction, amplitude drops down to 8 (a 20% reduction) due to higher overall damping.
- The bridge response is de-amplified, mainly due to the de-amplification of the free field ground response.

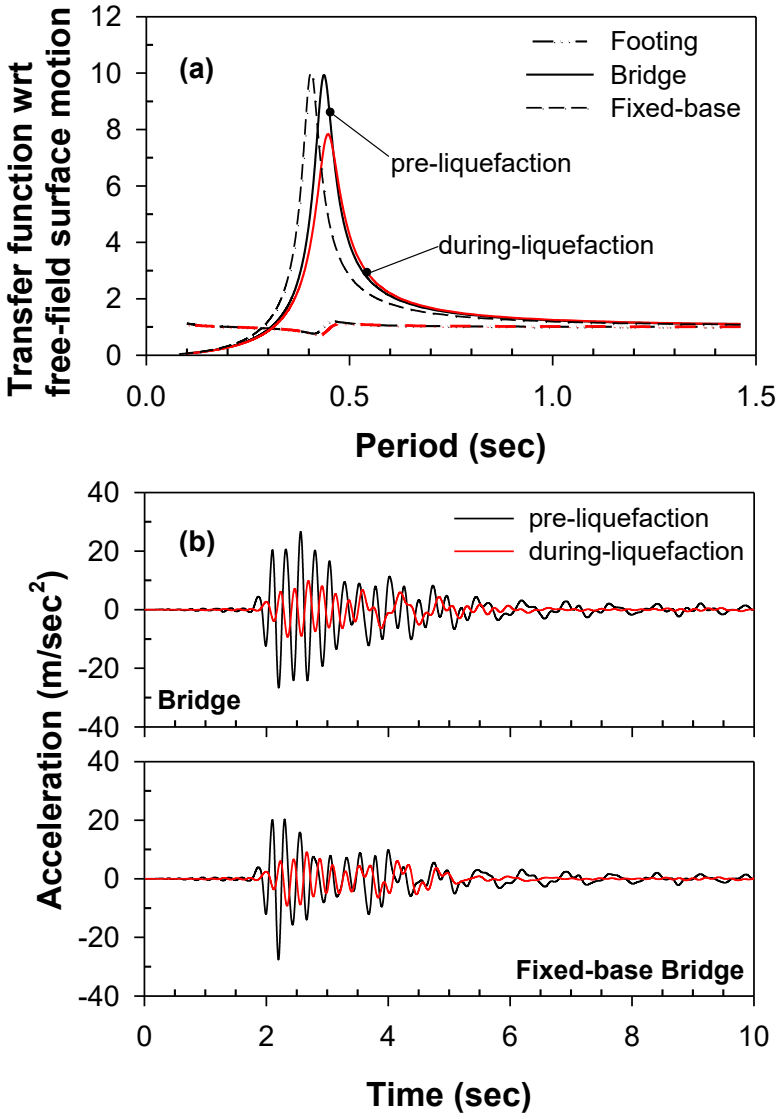

Fig. 13. Comparison of a) harmonic steady-state transfer functions and b) bridge acceleration history in pre- and during-liquefaction conditions; H_c = 5 m, B = 7 m, h_1 /B = 0.5, h_2 /B = 1, V_{s1} /V_{s2} = 5/3 (10).

5.4 Influence of thickness of the non-liquefiable surface crust

The influence of a thicker (h_1 = 7 m, V_{s1} = 100 m/s) surface zone on the vibrational characteristics of the bridge pier is presented in Fig.14, referring to a short pier. The following trends are worthy of note:

- The elongation of the fundamental period of the SSI system upon liquefaction is negligible.
- The decrease in bridge response amplification factor at resonance is significant, on the order of 40% over the pre-liquefaction case. However, the discrepancy is lower compared to the predicted one for h_1 = 3.5 m. This is anticipated as the thickness of the surface zone increases, hence liquefaction has a smaller influence on free-field response.
- Bridge acceleration histories show a substantial increase in response for the pre-liquefaction case and a decrease during liquefaction. This is understood given that the thickness of the soft soil overlying the stiff stratum doubles, thus the free-field motion is amplified. On the contrary, for liquefaction conditions the increase in thickness of the surface soft soil leads to an elongation in fundamental site period to T_1 = 2.16 s, thus generating a significant de-amplification in seismic response.

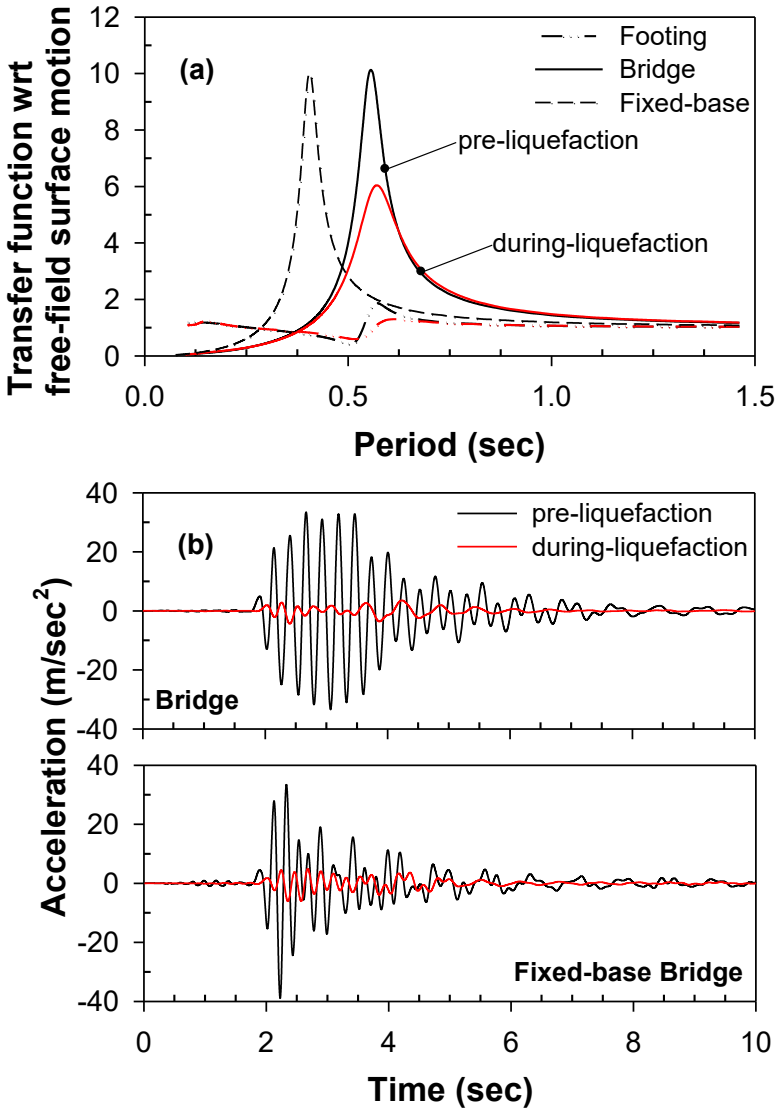

Fig. 14. Comparison of a) harmonic steady-state transfer functions and b) bridge acceleration history in pre- and during-liquefaction conditions; H_c = 5 m, B = 7 m, h_1 / B = 1, h_2 / B = 1, V_{s1} / V_{s2} = 2/3 (4).

5.5 Effect of depth to bedrock

Figure 15a shows results for the harmonic steady-state transfer functions for a short bridge pier (H_c = 5m) when the bedrock is located at a shallow depth. Results refer to a soil profile having (h_1 / B) = 0.5, (h_2 / B) = 1, (V_{s1} / V_{s2}) = 2/3, as in application 5.1, with the exception that the total depth of the soil profile is 20m.

- Evidently, transfer functions with reference to rock outcrop motion change drastically, and the fundamental period of the soil deposit increases from 0.35 s to 1.63 s due to the softening of the soil caused by liquefaction. The analytical solution also predicts T_1 = 0.35 s

and 1.64 s for pre- and during-liquefaction conditions, respectively. As a result, the de-amplification of the free-field acceleration is substantial (Fig.15b), which hence results in major attenuation of the bridge acceleration (not shown).

- Note that the fundamental period of the SFSI system (for both pre- and during-liquefaction conditions) is unaffected by the presence of the shallow bedrock as the dynamic impedance functions are hardly affected.
- It is mentioned that in case of a short soil profile, the role of SSI in the response of a structure is more pronounced. For pre-liquefaction conditions, the fixed-base bridge acceleration is about 55 m/s^2 and upon consideration of SSI reduces to 26 m/s^2, for during-liquefaction conditions the acceleration is about 6 m/s^2 and 3.4 m/s^2, respectively.
- In light of the above and with reference to the impact of liquefaction on the dynamic response of a structure, there are two important mechanisms. The first mechanism is associated with the elongation of the site period due to the softening of the soil, which indicates that the triggering of liquefaction may attenuate the seismic motion. The second mechanism lies in the shift in fundamental period of the pier-foundation-soil system, which may transfer the period of the system out of the predominant (harmful) frequency range of the earthquake excitation. In this example, the most important mechanism seems to be the first one, as no significant elongation in fundamental period of the system is observed. Nevertheless, the effect of the second mechanism may be more pronounced in case of a smaller footing. If one solves the problem at hand by utilizing a square footing of 5m wide (instead of 7m), the increase in fundamental period of the bridge pier is an appreciable 21%. This renders the second mechanism an important factor as well, which may affect the bridge response upon liquefaction. In this regard, it should be mentioned that period elongation increases the system deformations, as the fundamental period is shifted into the displacement-sensitive region of the spectrum. This may lead to midspan bridge collapse, a failure mechanism based on the differential elongation of fundamental period of piers supporting a river bridge due to liquefaction, and has been observed in many cases [39]. This means that upon the implementation of the proposed method the pier's lateral displacements should be always checked to be within acceptable limits.

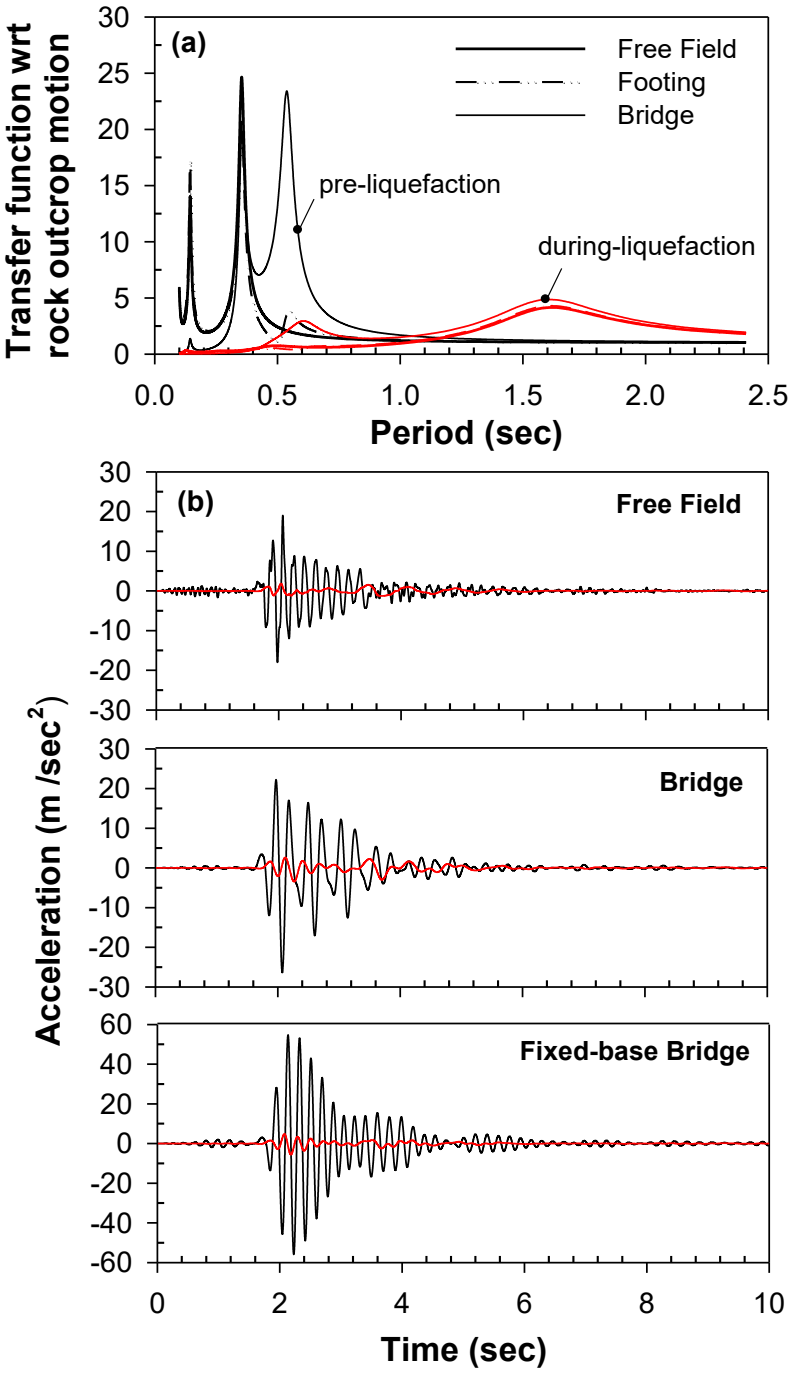

Fig. 15. Comparison of a) harmonic steady-state transfer functions and b) free-field and bridge acceleration history in pre- and during-liquefaction conditions for a short pier and shallow soil profile; H_c = 5 m, B = 7 m, h_1 / B = 0.5, h_2 / B = 1, V_{s1} / V_{s2} = 2/3 (4).

5.6 Bridge seismic response considering only static stiffness

Figure 16 presents results in case where the frequency-dependence of stiffness is ignored and only the static value is considered, i.e., stiffness for $\omega = 0$. Results refer to $(h_1 / B) = 0.5$, $(h_2 / B) = 1$, $(V_{s1} / V_{s2}) = 2/3$ (4) and $H_c = 5$ m, taking into account the horizontal and rocking

static stiffness (vertical stiffness is not part of the dynamic problem). The material damping ratio for both pre- and during-liquefaction conditions is assumed equal to 10%, being a more realistic value for a soft soil. For simplicity, in this example, radiation damping has been neglected.

- Evidently, the fundamental period of the pier-foundation-soil system does not shift, but the amplitude changes. It is observed that for both pre- and during-liquefaction conditions the amplification factor is relatively low, due to the assumed value of soil material damping (10%). Considering only static stiffness and no radiation damping, the decrease in amplitude is less than about 11%.
- The high peaks in footing harmonic transfer functions in the short period range is probably the result of a "secondary resonance" between the strong-short period part of the excitation motion and the resonance of the first soil layer (i.e., $4h_1 / V_{s1} = 4 \times 3.5/100 \cong 0.14$ s). However, the impact of this part of footing motion on bridge response is insignificant.
- Comparison of bridge acceleration history in pre- and during-liquefaction conditions shows that the bridge motion decreases under the effect of liquefaction, even without the beneficial effect of the frequency-dependent stiffness and damping of the footing. Overall, using static stiffness in the analysis of the specific problem may lead to conservative results.

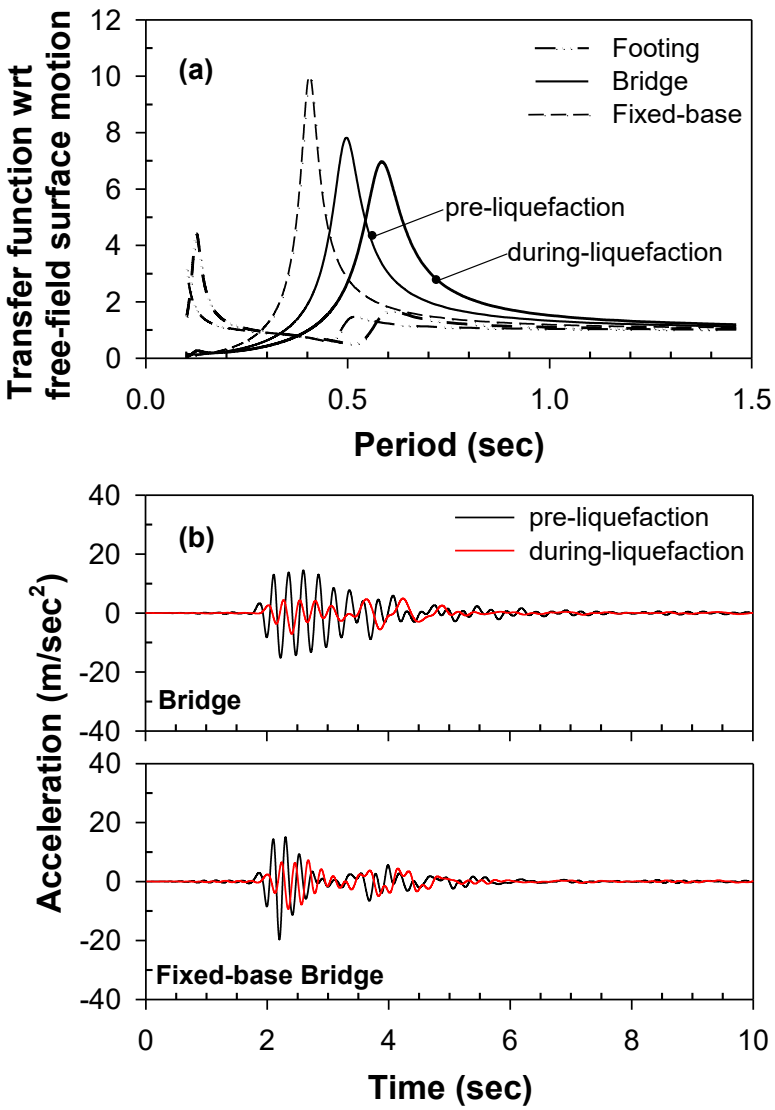

Fig. 16. Comparison of a) harmonic steady-state transfer functions and b) free-field acceleration history in pre- and during-liquefaction conditions considering only static stiffness; H_c = 5 m, B = 7 m, h_1 / B = 0.5, h_2 / B = 1, V_{s1} / V_{s2} = 2/3 (4).

5.7 Shift in natural period of the system upon liquefaction

As a final remark, one may quantify the influence of liquefaction on the natural period of the system by using the results for static stiffness of footing and rearranging Eq. (4) by means of the familiar equation of Veletsos and Meek [20, 44, 57]

$$\frac{T}{T_{st}} = \left\{1+\left[\frac{4\pi^2}{a_{hh}}\frac{\gamma}{H_c/B}\left(\frac{H_c}{T_{st}\,V_{s1}}\right)^2\right]\left[1+\frac{a_{hh}}{a_{rr}}\left(\frac{H_c}{B}\right)^2\right]\right\} \qquad (6)$$

with γ (= m_s /(ρ_1 H_c B^2)) being the relative mass density and a_{hh} (= K_{hh}/(G_1 B)) and a_{rr} (= K_{rr}/(G_1 B^3)) the dimensionless static stiffness coefficients. Fig. 17 depicts results for the relative natural period, $\tilde{T}_{liq}/\ \tilde{T}_{pre\text{-}liq}$, of the pier-foundation-soil system, obtained by dividing the right-hand side of Eq. 6 for the relevant conditions, as a function of the dimensionless ratio $H_c/(T_{st}\ V_{s1})$. Evidently, increase in (H_c/B) ratio and decrease in (h_1/h_2) result in a greater shift in the fundamental period of the system. This graph can be used to size the footing from a seismic isolation viewpoint.

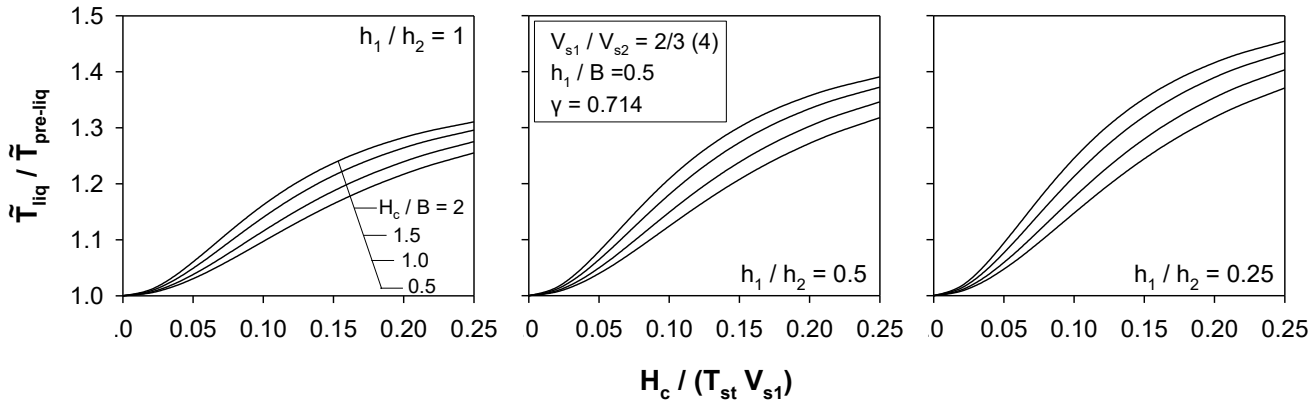

Fig. 17. Relative natural period of the system upon the influence of liquefaction.

6. Conclusions

The main conclusions of this study are:

1. Under the convenient assumption of equivalent material linearity, the dynamic impedance problem of a rigid square footing lying on a three-layer liquefiable soil profile was numerically investigated, considering all three planar oscillation modes (vertical, horizontal and rocking). Notwithstanding the non-linear nature of the liquefaction phenomenon, it was demonstrated that one may employ elastodynamic analysis as an engineering approximation to the problem in the sub-structuring sense, i.e., by assuming appropriate values for the shear wave velocity and material damping of the liquefied soil stratum, and considering a kind of "permanent" liquefied condition during the seismic event. This treatment facilitates the comparison between results during liquefaction and prior to liquefaction for the impedance functions of footing and the seismic response of bridge pier.

2. It is well known that such an approach may lead to inaccurate results when trying to simulate liquefaction, which involves strong nonlinearities, pore pressure effects, etc. On the other hand, a rough estimation of surface free-field motion in presence of liquefaction may be

possible through the viscoelastic assumption in an approximate manner, following the works in Refs. 7, 9, 54, which obtain surface elastic response spectra combining responses of the soil in the pre-liquefaction and during-liquefaction stages. In the same vein, it is possible to extrapolate these concepts to the structural response (i.e. furnishing a rule which combines two simple viscoelastic analyses to obtain the final spectrum). This is a worthy future research task, which will take considerable effort and caution to be completed as the aforementioned analyses are far more complicated (3D, elastoplastic, with soil and structural elements) than the 1D soil response analyses in Refs 7, 9 and 54. In addition, it is believed by the authors that the simplified visco-elastic analyses of this paper serve well the "proof-of-concept" aim of the present study.

3. Results obtained from simplified cone models (CONAN analysis) compare reasonably well with rigorous elastodynamic results for a three-layer profile using boundary elements (ISoBEM analysis) with deviations of about 20%. From a geotechnical engineering viewpoint, results are generally comparable and both methods demonstrate a significant decrease in footing stiffness accompanied by a considerable increase in damping due to liquefaction. In this light, the cone solution seems to be sufficient for a preliminary assessment of the problem.

4. Static stiffness of the footing drops dramatically under liquefied conditions. Based on the more rigorous BEM analyses, the decrease in static stiffness ranges from 11% to 84% for the vertical mode, 11% to 56% for the horizontal mode, and 1% to 59% for rocking. Using the BEM results, regression formulae for the vertical, horizontal and rocking static stiffness were obtained, which can be used for an initial assessment of the static stiffness of surface footings on liquefied soil.

5. The influence of liquefaction on the dynamic impedance functions is investigated through the dimensionless ratios ($\tilde{K}_{ij}$ / K_{ij}) and ($\tilde{C}_{ij}$ / C_{ij}). Results demonstrate the existence of two distinct regions: for the low frequency range and footings used for the foundation of common structures ($\omega h_1/V_{s1} < 1 \sim 2$), a significant reduction is observed in dynamic stiffness accompanied by a considerable increase in damping. Outside this range ($\omega h_1 / V_{s1} > 2$), dynamic stiffness exhibits sharp undulations while damping ratio ($\tilde{C}_{ij} / C_{ij}$) tends to unity.

6. Key parameters of the problem emerging from this study are the thickness of the surface non-liquefiable crust (h_1/B), the thickness of the liquefiable soil layer (h_2/B), the relative stiffness of the surface layer (V_{s1} /V_{s2}), and the dimensionless excitation frequency ($\omega h_1 / V_{s1}$).

7. The (h_1/B) ratio controls the undulations of the dimensionless ratios ($\tilde{K}_{ij} / K_{ij}$) and ($\tilde{C}_{ij} / C_{ij}$), and the change in the dynamic stiffness and damping due to liquefaction. On the other hand, The (h_2/B) and the (V_{s1}/V_{sliq}) ratios affect only marginally the variation in the dynamic impedance functions.

8. Upon liquefaction, the normalized static stiffness increases with increasing (h_1/B) and decreases with increasing (h_2/B) and increasing (V_{s1}/V_{sliq}).

9. To assess the impact of liquefaction on the dynamic response of the bridge pier, two separate analyses prior and during liquefaction were employed. In the frequency domain, results reveal elongation in the fundamental period of the SSI system and drop in amplification factor due to liquefaction. Time-history analyses showed significant attenuation of both the free-field and the bridge motion.

10. In case of tall bridge piers, liquefaction does not significantly modify the vibrational characteristics of the SFSI system. A small shift in the fundamental period of the system and a marginal decrease in amplitude are observed, while the peak acceleration developing on the bridge seems to be unaffected.

11. The stiffness of the non-liquefiable surface crust plays a significant role in the dynamic response of the pier-foundation-soil system. A stiff zone appears to act as a fixity condition for the pier and, hence, the fundamental period of the system is close to the fixed-base value. Nevertheless, the bridge response is de-amplified due to the softening of the soil deposit.

12. As the thickness of the surface crust increases, the elongation of the fundamental period of the system is marginal, while the decrease in system amplitude at resonance is decisive. Moreover, the increase in thickness of the surface soft soil leads to a lengthening in fundamental site period, which further contributes to the de-amplification of seismic response in both soil and structure.

13. Since engineers commonly use static foundation stiffness (instead of the actual frequency-dependent impedance functions) for design purposes, the consequences of this practice were examined. Zero radiation damping and the same soil material damping were assumed for both pre- and during-liquefaction conditions. Apparently, the fundamental period of the system is unaffected. However, the beneficial effect of the enhanced damping of the liquefied soil was not considered, leading to conservative results. Nevertheless, during liquefaction, the bridge motion decreases due to the softening of the soil that controls the free field response.

14. Liquefaction has a threefold impact on pier response. The first mechanism is associated with the elongation of the site period due to the softening of the soil, which indicates that the triggering of liquefaction may attenuate the seismic motion. The second mechanism refers to the increase in damping during liquefaction, which also dissipates seismic energy leading to a reduced free-field motion. The third mechanism relates to the shift in fundamental period of the pier-foundation-soil system, which may bring the period of the system out of the harmful frequency range of the earthquake excitation. In principle, all three mechanisms may play an important role in the modification (decrease) of seismic response during liquefaction. However, the effect of soil liquefaction on the vibrational characteristics of the pier-foundation system decreases drastically with increasing soil crust thickness and, consequently, the intended natural base isolation of the structural system is mainly achieved by the reduction in free-field seismic ground response.

It is finally noted that, contrary to common liquefaction-related hazards (e.g. lateral spreading, settlement, etc.) where a statistically minimum value of the liquefaction resistance (CRR) is used to define FSL, the proposed design concept relies upon the occurrence of liquefaction and consequently it should be based on a statistically maximum CRR value. It will not be difficult to modify the empirical charts that are presently used for this purpose, based on the probabilistic evaluation of the corresponding field data, e.g. instead of considering the liquefaction resistance with 95% probability of exceedance we should consider the one with 5% probability of exceedance [35]. Until then, liquefaction evaluation, in connection to the present problem, should be based on the "un-conservative" (in the common sense of the term) selection of soil parameters, e.g. choose the Nspt and qcpt values with probability 95% of not being exceeded.

Appendix A

Predictive equations for the static stiffness of a surface square rigid footing on liquefied soil:

1. Vertical static stiffness

For $h_2/B = 0.5$,

$$\frac{K_{vv}^{0}}{G_1 B} = -0.28 + 8.34 Exp\left[-0.33\frac{V_{s1}}{V_{sliq}}\right] + \left(1 - Exp\left[-1.2\frac{h_1}{B}\right]\right)\left\{-6.82 + 10.15\left(1 - Exp\left[-0.54\frac{V_{s1}}{V_{sliq}}\right]\right)\right\} \quad (A.1)$$

For $1 \le h_2/B \le 2$,

$$\frac{K_{vv}^{0}}{G_1 B}=\left(1.54-0.27\frac{h_2}{B}\right)\left\langle\left(-0.174+2.33Exp\left[-0.254\frac{V_{s1}}{V_{sliq}}\right]\right)+\right.$$
$$\left.+\left\{\left(2.24+2.84\frac{h_2}{B}\right)\left(1-Exp\left[-\left(0.72-0.21\frac{h_2}{B}\right)\frac{h_1}{B}\right]\right)-\left(2.04-0.15\frac{h_2}{B}\right)\left(1-Exp\left[-\left(0.05+0.46\frac{h_2}{B}\right)\frac{h_1}{B}\right]\right)\right\}\right\rangle$$

(A.2)

2. Horizontal static stiffness

$$\frac{K_{hh}^{0}}{G_1 B}=\left[1.07-0.18\frac{h_2}{B}+0.07\left(\frac{h_2}{B}\right)^2\right]\times$$
$$\times\left\langle\left(0.32+2.46\times Exp\left[-0.32\frac{V_{s1}}{V_{sliq}}\right]\right)+2.1\times\left(1-Exp\left[-0.55\frac{V_{s1}}{V_{sliq}}\right]\right)\left\{1-Exp\left[-\frac{h_1}{B}\left[2.02-0.83\left(\frac{h_2}{B}\right)^{0.45}\right]\right]\right\}\right\rangle$$

(A.3)

3. Rocking static stiffness

$$\frac{K_{rr}^{0}}{G_1 B^3}=0.01+\frac{1}{1.26+0.006\left(V_{s1}/V_{sliq}\right)}\left\{1-Exp\left[-\frac{h_1}{B}\left(\frac{1}{0.37+0.024\,V_{s1}/V_{sliq}}-\frac{1}{1.68+0.28\,V_{s1}/V_{sliq}}\frac{h_2}{B}\right)\right]\right\}$$

(A.4)

Appendix B

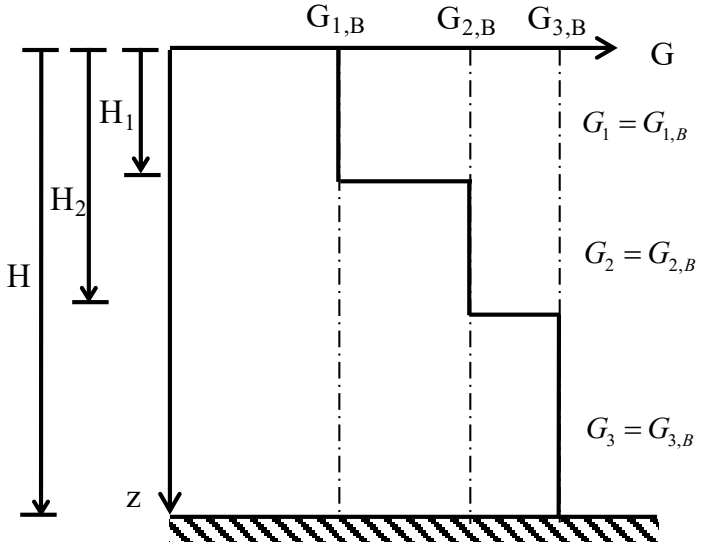

Fig. B1. Inhomogeneous three-layer soil deposit over a rigid base.

Fig. B1 illustrates a three-layer soil deposit over a rigid base. The mass density and the shear modulus are assumed constant within each layer, with G_B being the shear modulus at the bottom of the layer and z the depth measured from the ground surface.

Based on [17, 42] the natural frequencies of a soil deposit may be derived using the Rayleigh quotient which, upon expressing the displacement as $u(z) = u_0\,\psi(z)$, becomes

$$\omega^2 = \int_0^H G(z)u'(z)^2\,dz \Big/ \int_0^H \rho u(z)^2 = \int_0^H G(z)\psi'(z)^2\,dz \Big/ \int_0^H \rho\psi(z)^2 \tag{B1}$$

$\psi(z)$ being a dimensionless unitary shape function representing the shape mode corresponding to the fundamental natural frequency of the inhomogeneous soil. The mode shape is determined as the lateral movement of the soil column under distributed load, with the origin of displacement axis at the top of the soil column. The soil lateral displacement is

$$u(z) = \int_0^z \gamma(z)\,dz = \int_0^z \frac{\rho(z)g\,z}{G(z)}\,dz \tag{B2}$$

where $\gamma(z)$ is the shear strain. The shape function is usually unitary and should be zero at the base, to satisfy the essential boundary conditions of the problem,

$$\psi(z) = 1 - \int_0^z \frac{\rho(z)g\,z}{G(z)}\,dz \Big/ \int_0^H \frac{\rho(z)g\,z}{G(z)}\,dz \tag{B3}$$

Specific forms of the above equation, for the single layer and the two-layer soil profile, are provided in [17]. For a three-layer soil deposit with each layer having constant shear modulus, Eq. B3 becomes

$$\psi(z) = \frac{1}{D}\begin{cases} \dfrac{\tilde{H}_1^2 - \tilde{z}^2}{2} + a_1\dfrac{\tilde{H}_2^2 - \tilde{H}_1^2}{2} + a_2\dfrac{1-\tilde{H}_2^2}{2}, & 0 \le \tilde{z} \le \tilde{H}_1 \\ a_1\dfrac{\tilde{H}_2^2 - \tilde{z}^2}{2} + a_2\dfrac{1-\tilde{H}_2^2}{2}, & \tilde{H}_1 \le \tilde{z} \le \tilde{H}_2 \\ a_2\dfrac{\left(1-\tilde{z}^2\right)}{2}, & \tilde{H}_2 \le \tilde{z} \le 1 \end{cases} \tag{B4}$$

with $\tilde{H}_1 = H_1/H$ and $\tilde{H}_2 = H_2/H$ being the dimensionless depth of the first and second layer of the soil deposit, $\tilde{z} = z/H$ is the dimensionless depth measured from ground surface, and

$$D = \frac{\tilde{H}_1^2}{2} + a_1\frac{\tilde{H}_2^2 - \tilde{H}_1^2}{2} + a_2\frac{1-\tilde{H}_2^2}{2} \tag{B5}$$

$$a_1 = \left(V_{s1,B}/V_{s2,B}\right)^2, \quad a_2 = \left(V_{s1,B}/V_{s3,B}\right)^2 \tag{B6}$$

with $V_{s,B} = (G_B/\rho)^{1/2}$ being the shear wave propagation velocity at the bottom of the layer.

Using the shape function in Eq. B4, the Rayleigh quotient (Eq. B1) yields

$$\omega_n^2 = \frac{k_1 + a_1^{-1}\zeta_1 k_2 + a_2^{-1}\zeta_2 k_3}{k_4 + \zeta_1 k_5 + \zeta_2 k_6}\left(\frac{V_{s1,B}}{H}\right)^2 \tag{B7}$$

where

$$k_1 = \frac{H_1^3}{3} \quad , \quad k_2 = a_1^2\frac{H_2^3 - H_1^3}{3} \quad , \quad k_3 = a_2^2\frac{1 - H_2^3}{3} \tag{B8}$$

$$k_4 = \frac{2H_1^5}{15} - \frac{H_1^3}{3}\left[a_1\left(H_1^3 - H_2^3\right) - a_2\left(1 - H_2^3\right)\right] + \frac{H_1^4}{4}\left[a_1\left(H_1^3 - H_2^3\right) - a_2\left(1 - H_2^3\right)\right]^2 \tag{B9}$$

$$\begin{aligned} k_5 = -\frac{1}{60}\left(H_1^4 - H_2^4\right)\Big[&10a_1a_2\left(H_1^4 - H_2^4\right)\left(H_1^4 + 2H_2^4\right)\left(-1 + H_2^3\right) + 15a_2^2\left(-1 + H_2^3\right) + \\ &+ a_1^2\left(H_1^4 - H_2^4\right)^2\left(3H_1^6 + 9H_1^4H_2^4 + 8H_2^6\right)\Big] \end{aligned} \tag{B10}$$

$$k_6 = -\frac{a_2^2}{60}\left(-1 + H_2^3\right)^3\left(8 + 9H_2^4 + 3H_2^6\right) \tag{B11}$$

$$\zeta_1 = \rho_2/\rho_1 \quad , \quad \zeta_2 = \rho_3/\rho_1 \tag{B12}$$

Acknowledgements

This research was co-financed by the European Union (European Social Fund – ESF) and Greek national funds through the Operational Program "Education and Lifelong Learning" of the National Strategic Reference Framework (NSRF) - Research Funding Program: THALES. Investing in knowledge society through the European Social Fund. The help of Professors Demosthenes Polyzos and Dimitri Beskos of UPatras in making available ISoBEM software to the authors is gratefully acknowledged, as well as the help of Professor Stephanos Tsinopoulos of the Technological Institute of Patras in using the software. The authors also benefitted from discussions with Professor Anastasios Sextos and Dr. Dimitris Karamitros of Bristol University.

References

[1] Acacio, A., Kobayashi, Y., Towhata, I., Bautista, R., Ishihara, K., (2001). Subsidence of building foundation resting upon liquefied subsoil; Case studies and assessment. *Soils Found (JGS)*;41(6); 111-128.

[2] Adachi, T., Iwai, S., Yasui, M. Sato, Y. (1992). Settlement and inclination of reinforced concrete buildings in Dagupan City due to liquefaction during 1990 Philippine Earthquake, *Proceedings, 10WCEE,* Balkema Rotterdam, 2; 147-152.

[3] Ahmad, S., Bharadwaj, A. (1991). Horizontal impedance of embedded strip foundations in layered soil. *J Geotech Eng*;117;1021-41.

[4] Ahmad, S., Rupani, A. (1999). Horizontal impedance of square foundation in layered soil. *Soil Dyn Earthq Eng*;18(1);59-69.

[5] Anoyatis, G. and Mylonakis, G. (2012). Dynamic Winkler modulus for axially loaded piles. *Geotechnique*; 62;521-536.

[6] Bouckovalas, G.D., Karamitros D.K., Madabhushi, S.P.G. et al. (2015). FLIQ: Experimental Verification of Shallow Foundation Performance under Earthquake-induced Liquefaction. *Geotech, Geolog Earthq Eng*, 35;525-542.

[7] Bouckovalas, G**.,** Tsiapas, Y., Theocharis, A., Chaloulos, Y., (2016). Liquefied ground response: Seismic isolation or amplification? *Soil Dyn Earthq Eng*; 91;329-339.

[8] Bouckovalas G., Psycharis I. et al. (2017). Performance-based design of bridge piers in liquefiable sites with shallow foundation and limited ground improvement. *PBDIII: Performance Based design in Geotech Earthq Eng*, Vancouver, July 16-19.

[9] Bouckovalas, G. D., Tsiapas, Y. Z., Zontanou, V. A., Kalogeraki, C. G. (2017). Equivalent linear computation of response spectra for liquefiable sites: The spectral envelope method. *J Geotech Geoenv Eng (ASCE)*;143(4):04016115.

[10] Bray J. and Macedo J. (2017). 6th Ishihara Lecture: Simplified procedure for estimating liquefaction-induced building settlement*. Soil Dyn Earthq Eng*;102;215-231.

[11] Buckingham E. (1914). On physically similar systems; illustrations of the use of dimensional equations. *Physical Review*;4(4);345-376.

[12] Coehlo, P., Haigh, S.K, Madabushi, S.P.G. (2005). Development, effects and mitigation of earthquake induced liquefaction: A comprehensive study based on dynamic centrifuge modeling, *Proceedings, 16th International Conf on SMGE*, Osaka, Japan.

[13] Dashti, S., Bray, J., Riemer, M., Wilson, D. (2008). Centrifuge experimentation of building performance on liquefied ground, *Geotechnical Special Publication*, 181.

[14] Dashti S., Bray J.D., Pestana J.M., Riemer M., Wilson D. (2010a). Centrifuge Testing to Evaluate and Mitigate Liquefaction-Induced Building Settlement Mechanisms. *J Geotech Geoenv Eng*; 136(7);918-929.

[15] Dimitriadi V.E., Bouckovalas G.D., Papadimitriou A.G. (2017). Seismic performance of strip foundations on liquefiable soils with a permeable crust. *Soil Dyn Earthq Eng*; 100;396-409.

[16] Dimitriadi V.E., Bouckovalas G.D., Chaloulos Y.K., Aggelis A.S. (2018). Seismic liquefaction performance of strip foundations: Effect of ground improvement dimensions. *Soil Dyn Earthq Eng*;106;298-307.

[17] Durante, M. G., Karamitros, D., Di Sarno, L., et al. (2015). Characterization of shear wave velocity profiles of non-uniform bi-layer soil deposits: Analytical evaluation and experimental validation. *Soil Dyn Earthq Eng*; 75;44-54.

[18] Farrell, T. M. and Kutter, B. L. (1993). *Experimental results of Model No 12, Verifications of Numerical Procedures for the Analysis of Soil Liquefaction Problems*, Balkema, Rotterdam, ISBN 90 5410 360 4.

[19] Gazetas, G. (1991). Formulas and charts for impedances of surface and embedded foundations. J Geotech Eng (ASCE);117 (9);1363-1381.

[20] Givens, M. J., Mylonakis, G., & Stewart, J. P. (2016). Modular analytical solutions for foundation damping in soil-structure interaction applications. Earthquake Spectra, 32(3), 1749-1768. DOI: 10.1193/071115EQS112M.

[21] Hatzigeorgiou, G. and Beskos, D. (2011). Dynamic inelastic structural analysis by the BEM: A review. *Engineering Analysis with Boundary Elements*. 35(2). 159-169. 10.1016/j.enganabound.2010.08.002.

[22] Heidarzadeh, B., Mylonakis, G., Stewart, J.P. (2015). Stresses beneath dynamically applied vertical point loads. *6th International Conference on Earthquake Geotechnical Engineering ICEGE*, Christchurch, New Zealand.

[23] Hiltunen, D., Dunn, P., Toros, U. (2007). Cone model predictions of dynamic impedance functions of shallow foundations. *4th International Conference on Earthquake Geotechnical Engineering ICEGE*, Thessaloniki, Greece.

[24] Ishihara, K., Acacio, A., Towhata, I. (1993). Liquefaction-induced Ground Damage in Dagupan in the July 16, 1990 Luzon Earthquake, *Soils and Foundations*, 33(1), 133-154.

[25] ISoBEM: Boundary Element Method Package. http://bemsands.com, 2012.

[26] Karamitros, D. K., Bouckovalas, G. D., Chaloulos, Y. K. (2013a). Insight into the seismic liquefaction performance of shallow foundations. *J Geotech Geoenv Eng (ASCE)*;139(4);599-607.

[27] Karamitros, D. K., Bouckovalas, G. D., Chaloulos, Y. K. (2013b). Seismic settlements of shallow foundations on liquefiable soil with a clay crust. *Soil Dyn Earthq Eng*;46;64-76.

[28] Karamitros, D. K., Bouckovalas, G. D., Chaloulos, Y. K, Andrianopoulos, K. I. (2013c). Numerical analysis of liquefaction-induced bearing capacity degradation of shallow foundations on a two-layered soil profile. *Soil Dyn Earthq Eng*;44;90-101.

[29] Karatzia, X. (2016). Theoretical investigation of geotechnical seismic isolation of bridge piers on footings and piles. *Doctoral Dissertation*, Dept of Civil Eng, UPatras, Greece.

[30] Karatzia, X., Mylonakis, G., Bouckovalas, G., (2017a). 3D Dynamic impedances of surface footings on liquefiable soil: equivalent linear approach. *16th World Conference on Earthquake Engineering WCEE*, Santiago, Chile.

[31] Karatzia, X., Mylonakis, G., Bouckovalas, G., (2017b). Equivalent-Linear Dynamic Stiffness of Surface Footings on Liquefiable Soil. *6th Int Conf on Computational Methods in Structural Dyn and Earthq Eng COMPDYN*, Rhodes Island, Greece.

[32] Kawasaki, K., Sakai, T., Yasuda, S., Satoh, M. (1998). Earthquake induced settlement of an isolated footing for power transmission tower, Centrifuge 98, 271-276.

[33] Kokusho, T. (2014). Seismic base-isolation mechanism in liquefied sand in terms of energy. *Soil Dyn Earthq Eng*, Elsevier BV, 63, 92–97.

[34] Lesgidis, N., Kwon, O., Sextos, A. (2015). A time-domain seismic SSI analysis method for inelastic bridge structures through the use of a frequency-dependent lumped parameter model. *Earthquake Engineering & Structural Dynamics*. 10.1002/eqe.2573.

[35] Liao, S.S.C., Veneziano, D., Whitman, R.V. (1988). Regression models for evaluating liquefaction probability. *J Geotech Eng*, ASCE, 114(4);389-411.

[36] Lombardi D. and Bhattacharya S. (2014). Modal analysis of pile-supported structures during seismic liquefaction. *Earthq Eng Struct Dyn;* 43 (1), 119-138, 10.1002/eqe.2336.

[37] Meek, J. W., Wolf, J. P. (1992). Cone models for soil layer on rigid rock. *J Geotech Eng (ASCE)*;118;686–703.

[38] Miwa, S. and Ikeda, T. (2006). Shear modulus and strain of liquefied ground and their application to evaluation of the response of foundation structures. *Structural Engineering/Earthquake Engineering (JSCE)*;23(1);167-179.

[39] Mohanty P., Dutta S. C., Bhattacharya S. (2017). Proposed mechanism for mid-span failure of pile supported river bridges during seismic liquefaction. *Soil Dyn Earthq Eng*;102;41-45, 10.1016/j.soildyn.2017.08.013

[40] Mylonakis, G. (1995). SFIAB (computer code for academic use).

[41] Mylonakis, G., Nikolaou, S., Gazetas, G. (2006). Footings under seismic loading: Analysis and design issues with emphasis on bridge foundations. *Soil Dyn Earthq Eng*; 26(9);824-853.

[42] Mylonakis, G., Rovithis, E., Parashakis, H. (2013). 1D harmonic response of layered inhomogeneous soil: Exact and approximate analytical solutions. *Computational Methods in Earthq Eng; Computational methods in Applied Sciences*;30;1-32.

[43] Naesgaard, E., Byrne, P.M., Ven Huizen, G. (1998). Behavior of light structures founded on soil 'crust' over liquefied ground, *Geotech Earthq Eng & Soil Dyn III, Proceedings of a Specialty Conference*, 1, 422-434.

[44] NIST (2012). Soil-Structure Interaction for Building Structures, GCR 12-917-21, prepared by the NEHRP Consultants Joint Venture, a partnership of the Applied Technology Council and the Consortium for Universities for Research in Earthquake Engineering, for the National Institute of Standards and Technology, Gaithersburg, MD.

[45] Pais, A. and Kausel, E. (1988). Approximate formulas for dynamic stiffnesses of rigid foundations. *Soil Dyn Earthq Eng*;7(4);213–227.

[46] Pease, J. W., and O'Rourke, T. D. (1997). "Seismic response of liquefaction sites." J. Geotech. Geoenviron. Eng, 10.1061/(ASCE)1090-0241(1997)123:1(37), 37-45.

[47] Pender, M. J. (2018). Earthquake inertia effects on shallow foundation bearing strength. *Géotechnique*, 68(7); 640-645, 10.1680/jgeot.17.T.006.

[48] Pitilakis, D., Moderessi-Farahmand-Razavi, A., Clouteau, D. (2013). Equivalent-Linear Dynamic Impedance Functions of Surface Foundations. *J Geotech Geoenv Eng*, 139(7); 1130-1139, 10.1061/(ASCE)GT.1943-5606.0000829.

[49] Polyzos, D., Tsinopoulos, S., Beskos, D. (1998). Static and dynamic boundary element analysis in incompressible linear elasticity. *European Journal of Mechanics A/Solids*; 17(3);515-536.

[50] Sextos, A., Psilla, N., Psycharis, I. et al (2014). Performance criteria for bridges designed with spread footings on liquefiable soils. *2nd European Conference on Earthquake Engineering and Seismology*, Istanbul, Turkey, Aug. 25-29.

[51] Sitar, N. and Hausler, E. (2012). Influence of ground improvement on liquefaction induced settlements: observations from case histories and centrifuge experiments. *Invited Lecture presented to the Korean Geotechnical Society*, Seoul, Korea, March 22.

[52] Spyrakos, C. C. and Xu, C. J. (2004). Dynamic analysis of flexible massive strip-foundations embedded in layered soils by hybrid BEM-FEM. *Computers & Structures*; 82(29–30);2541–2550.

[53] Theocharis, A. (2011). Numerical analysis of liquefied ground response under harmonic seismic excitation-Variable thickness of liquefied layer. *Diploma thesis*, NTUA, Greece.

[54] Tsiapas, Y. and Bouckovalas, G. (2019). "Equivalent linear computation of response spectra for liquefiable sites: The spectral interpolation method." *Soil Dyn Earthq Eng*;116;541-551.

[55] Tsinopoulos, S., Kattis, S., Polyzos, D., Beskos D. (1999). An advanced boundary element method for axisymmetric elastodynamic analysis. *Computer Methods in Applied Mechanics and Engineering*;175;53-70.

[56] Vassilopoulou, I., Kaymenaki, V., Gantes, Ch., and Bouckovalas G. (2017). Criteria for Preliminary Design of an Arched Steel Bridge on Shallow Foundation under Soil Liquefaction Conditions. *The Open Civil Engineering Journal*, 11 (Suppl.-5, M10), 1170-1190

[57] Veletsos, A. S. and Meek, J. W. (1974). Dynamic behavior of building-foundation systems. *Earthq Eng Struct Dyn*; 3(2);121–138.

[58] Vrettos, C. (1999). Vertical and rocking impedances for rigid rectangular foundations on soils with bounded non-homogeneity. *Earthq Eng Struct Dyn*; 28(12);1525-1540.

[59] Wong, H. L. and Luco, J. E. (1985). Tables of impedance functions for square foundation on layered media. *Soil Dyn Earthq Eng*; 4(2);64–81.

[60] Wolf, J P. (1994). *Foundation vibrations analysis using simple physical models*. Prentice Hall.

[61] Wolf, J P. and Deeks, A.J. (2004). *Foundation Vibration Analysis: A Strength-of-Materials Approach*. Elsevier, Oxford, UK.

[62] Youd, T. L., and Carter, B. L. (2005). Influence of soil softening and liquefaction on spectral acceleration. *J Geotech Geoenv Eng*, 10.1061/(ASCE)1090-0241(2005)131:7 (811), 811-825.